

**AUGUST,2012**

**M.Sc in Civil Engineering**

**ÖMER FARUK ÖZKAPLAN**

**UNIVERSITY OF GAZIANTEP  
GRADUATE SCHOOL OF  
NATURAL & APPLIED SCIENCES**

**SIMULATION OF TEMPORAL LOCAL SCOUR  
BENEATH HORIZONTAL JETS BY A 3-PHASE CFD  
MODEL**

**M. Sc. THESIS  
IN  
CIVIL ENGINEERING**

**ÖMER FARUK ÖZKAPLAN  
AUGUST 2012**

**Simulation of Temporal Local Scour Beneath Horizontal  
Jets by A 3-Phase Cfd Model**

**University of Gaziantep**

**A Master Thesis in**

**Civil Engineering**

**Supervisor**

**Assoc. Prof. Dr. Aytaç GÜVEN**

**Ömer Faruk ÖZKAPLAN**

**August 2012**

©2012 Ömer Faruk ÖZKAPLAN

REPUBLIC OF TURKEY  
UNIVERSITY OF GAZİANTEP  
GRADUATE SCHOOL OF NATURAL & APPLIED SCIENCES  
(CIVIL ENGINEERING DEPARTMENT)

Name of the thesis: Simulation of Temporal Local Scour Beneath Horizontal Jets By  
A 3-Phase Cfd Model


Name of the student: Ömer Faruk ÖZKAPAN

Exam date: 15-08-2012

Approval of the Graduate School of Natural and Applied Sciences

  
Prof. Dr. Ramazan KOÇ  
Director

I certify that this thesis satisfies all the requirements as a thesis for the degree of  
Master of Science/Doctor of Philosophy.

  
Prof. Dr. Mustafa GÜNAL  
Head of Department

This is to certify that we have read this thesis and that in our consensus/majority  
opinion it is fully adequate, in scope and quality, as a thesis for the degree of Master  
of Science.

  
Assoc. Prof. Dr. Aytaç GÜVEN  
Supervisor


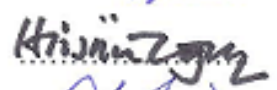

Examining Committee Members

Prof. Dr. Mustafa GÜNAL

Asst. Prof. Dr. Hüsnü UĞUR

Assoc. Prof. Dr. Aytaç GÜVEN

Signature

**I hereby declare that all information in this document has been obtained and presented in accordance with academic rules and ethical conduct. I also declare that, as required by these rules and conduct, I have fully cited and referenced all material and results that are not original to this work.**

**Ömer Faruk ÖZKAPLAN**

## **ABSTRACT**

### **SIMULATION OF TEMPORAL LOCAL SCOUR BENEATH HORIZONTAL JETS BY A 3-PHASE CFD MODEL**

ÖZKAPLAN, ÖmerFaruk

M.Sc. Thesis in Civil Eng.

Supervisor: Assoc. Prof.Dr.Aytaç GÜVEN

August 2012

60 page

In this study, a two dimensional time-dependent numerical model is proposed for simulation of temporal local scour profile and flow characteristics beneath horizontal turbulent jets downstream of rigid apron. The temporal scour profile was simulated by a 3-phase mixture (air, water, sand) model. The Renormalized Group (RNG)  $k-\epsilon$  turbulence model is used as a closure model. The flow conditions are assumed as unsteady. A two dimensional virtual numerical flume was composed using FLUENT CFD package. The Navier-Stokes equations for incompressible and viscous fluids were discretized by using finite volume method. The proposed numerical scheme was run for different experimental conditions recorded by others. Comparison of the proposed numerical model's predictions to the observed ones showed a good agreement which is an indication of the precision of the proposed numerical scheme. The overall results encouraged the use of the present model in simulation of movable (erodible) bed profiles beneath turbulent water jets.

**Key Words:** scour; turbulent jet; numerical modelling; flume; simulation; flow characteristic; local scour;  $k-\epsilon$  model

## ÖZ

### 3 FAZLI CFD MODELDE GEÇİCİ YEREL OYULMANIN SİMÜLASYONU

ÖZKAPLAN, Ömer Faruk

Yüksek Lisans Tezi, İnşaat Müh. Bölümü

Tez Yöneticisi: Doç. Dr. Aytaç GÜVEN

Ağustos 2012

60 sayfa

Bu çalışmada geçici lokal oyulma profili ve rijit zeminin mansabındaki yatay türbülanslı jetin altındaki akım karakteristiklerinin simülasyonu için 2 boyutlu zamana bağlı bir sayısal model sunulmuştur. Geçici yerel oyulma profili 3 fazlı bir karışım modeli ile (hava,su,kum) simule edilmiştir. Bir yaklaşım modeli olarak RNG k- $\epsilon$  türbülans modeli kullanılmıştır. Akış koşulları kararsız (unsteady) olarak öngörülmüştür. FLUENT CFD yazılım paketi kullanılarak sanal 2 boyutlu bir kanal tasarlanmıştır. Sıkıştırılamaz ve viskoz akışlar için Navier-Stokes denklemleri sonlu hacimler metodu kullanılarak diskritize edilmiştir. Başkaları tarafından kaydedilen farklı deneysel koşullar için sunulan sayısal şema çalıştırılmıştır. Önerilen sayısal modelin tahminlerinin gözlenenlerle kıyaslanması, önerilen sayısal şemanın hassaslığının bir göstergesi olduğunu göstermiştir. Bütün sonuçlar, türbülanslı su jetleri altındaki aşınabilir yatak profillerinin simülasyonunda mevcut modelin kullanılmasını teşvik etmiştir.

**Anahtar Kelimeler:** oyulma; çalkantılı jet; sayısal modelleme; kanal; simülasyon; akım karakteristikleri; yerel oyulma; k- $\epsilon$  modeli

***To My Family...***



## **ACKNOWLEDGEMENTS**

I would like to gratefully acknowledge the enthusiastic supervision of Assoc.Prof.Dr. Aytaç Güven during this work.

Special thanks to Head Department of Civil Engineering of University of Gaziantep Prof.Dr. Mustafa GÜNAL for his professional advices for my work.

I am thankful to the Advt. M.Emin ÖZKAPLAN for her important comments and recommendations about my thesis.

Lastly, I am also grateful to my family who encouraged me to pursue this topic and spent extra time helping me to achieve a clearer structure.

## TABLE OF CONTENTS

LIST OF FIGURES .....	viii
LIST OF TABLES .....	x
CHAPTER 1 .....	1
INTRODUCTION .....	1
1.1. General .....	1
1.2. Local Scour .....	2
1.2.1. Mechanism of scour by turbulent jet.....	2
1.2.2. Local scour beneath horizontal jet .....	3
1.2.2.1. Scouring Process .....	3
1.2.2.2. Effect of the jet entering movable bed .....	3
1.2.3. Result of scour hole forming.....	5
CHAPTER 2 .....	6
LITERATURE SURVEY .....	6
2.1.Application of RNG k- $\epsilon$ model .....	6
2.2.RANS k- $\epsilon$ model .....	7
2.3.Other Models.....	8
CHAPTER 3 .....	12
NUMERICAL MODEL AND GOVERNING EQUATIONS .....	12
3.1.Turbulence model.....	12
3.2.The k- $\epsilon$ Turbulence Model.....	12
3.2.1.Stardart k- $\epsilon$ Turbulence Model .....	13
3.2.2.RNG k- $\epsilon$ Turbulence Model.....	14
3.2.3.Realizable k- $\epsilon$ Turbulence Model .....	18
CHAPTER 4 .....	19
DESCRIPTION OF THE EXPERIMENTAL AND THE NUMERICAL MODELS .....	19
4.1. Description of the Experimental Model .....	19

4.2. The Numerical Model.....	20
4.2.1. Solution Method (GAMBIT AND FLUENT).....	21
4.2.1.1. GAMBIT .....	21
4.2.1.2. FLUENT .....	24
4.2.2. The Numerical Modelling Steps.....	25
4.2.2.1. Turbulence Modelling and Implementation of the Boundary Conditions .....	25
4.2.3. Time-Based Solution and the Convergence Criteria .....	26
CHAPTER 5 .....	27
RESULT AND DISCUSSION .....	27
CHAPTER 6 .....	39
CONCLUSIONS AND SUGGESTIONS FOR FURTHER RESEARCH .....	39
6.1. Conclusions .....	39
6.2. Suggestions For Further Research .....	40
REFERENCES .....	41

## LIST OF FIGURES

Figure 1.1 Local scour.....	4
Figure 4.1 Schematic drawing of scouring caused by jet.....	19
Figure 4.2 Defining vertexes using GAMBIT .....	22
Figure 4.3 Defining edges using GAMBIT.....	22
Figure 4.4 Defining faces using GAMBIT .....	23
Figure 4.5 Defining meshes using GAMBIT .....	23
Figure 4.6 Displaying the boundary conditions using GAMBIT.....	24
Figure 5.1 Fluent`s asymptotic scour profile vs. measured Adduce (2004)`sfor test 1.....	28
Figure 5.2 Fluent`s asymptotic scour profile vs. measured Adduce (2004)`s for test 2.....	28
Figure 5.3 Fluent`s asymptotic scour profile vs. measured Adduce (2004)`s for test 3.....	29
Figure 5.4 Fluent`s asymptotic scour profile vs. measured Adduce (2004)`s for test 4.....	29
Figure 5.5 The contours of volume fractions at initial stage.....	30
Figure 5.6 The contours of volume fractions of water phase for test 1 .....	30
Figure 5.7 The contours of volume fractions of sand phase for test 1 .....	31
Figure 5.8 The contours of volume fractions of water phase for test 2 .....	31
Figure 5.9 The contours of volume fractions of sand phase for test 2.....	31
Figure 5.10 The contours of volume fractions of water phase for test 3 .....	32

Figure 5.11 The contours of volume fractions of sand phase for test 3 .....	32
Figure 5.12 The contours of volume fractions of water phase for test 4 .....	32
Figure 5.13 The contours of volume fractions of sand phase for test 4.....	33
Figure 5.14 Distribution Fluent` <i>su</i> -velocity over the rigid apron and scour profile predictions for test 1 .....	33
Figure 5.15 Distribution Fluent` <i>sv</i> -velocity over the rigid apron and scour profile predictions for test 1 .....	34
Figure 5.16 Distribution Fluent` <i>su</i> -velocity over the rigid apron and scour profile predictions for test 3. ....	34
Figure 5.17 Distribution Fluent` <i>sv</i> -velocity over the rigid apron and scour profile predictions for test 3. ....	35
Figure 5.18 Predicted and observed $\sqrt{U'^2}/U_0$ distribution over the rigid apron and scour profile for test 1 .....	36
Figure 5.19 Predicted and observed $\sqrt{V'^2}/U_0$ distribution over the rigid apron and scour profile for test 1 .....	36
Figure 5.20 Predicted and observed $\sqrt{U'^2}/U_0$ distribution over the rigid apron and scour profile for test 3 .....	37
Figure 5.21 Predicted and observed $\sqrt{V'^2}/U_0$ distribution over the rigid apron and scour profile for test 3 .....	37

**LIST OF TABLES**

Table 4.1 Experimental conditions used in model validation ..... 20

# CHAPTER 1

## INTRODUCTION

### 1.1. General

The last few years, computers have become fast enough to make CFD computations applicable for engineering purposes. Some pilotage is needed on how to model different types of hydraulic structures. Sediment transport is a specific topic of hydraulic research. When a structure is made in a river, such as a bridge pier, a special flow pattern around the structure is formed. If the structure is made in a river with erodible bed, the water flow may lead to local scour around. This may again weaken the support for the construction. Local scour is a characteristic reason for bridge failures.

The purpose of the study is to offer a numerical model that predicts the depth and shape of the local scour hole using CFD package program called FLUENT. To assemble the turbulence some models will be used and evolved. These models are numerical methods developed to satisfy the closure of the time-averaged governing fluid flow equations by providing a scheme for the evaluation of the Reynolds stress terms. Present study for turbulence modelling, k- $\epsilon$  model will be used; it is the most widely used model of all the turbulence models. It is rated as a two equation model (Launder and Spalding, 1974). This represents the fact that the transport equation is solved for two turbulent quantities k and  $\epsilon$ . 2D Navier-Stokes equations will be used to demonstrate the flow in front of the breakwater. The standard k- $\epsilon$  model has been becoming more applied and well validated in local scour and sediment transport problems (Lu et al. 2005, Zhao et al. 2010, Cassan and Belaud 2011, Karim and Ali 2000. etc.). However, it still lacks the accuracy while modelling complex boundary flows such as temporal bed problems. Another version of k- $\epsilon$  model, namely, the Renormalized Group (RNG) k- $\epsilon$  model fulfils the requirements in this type of flow conditions. Hence, in this study, the RNG k- $\epsilon$  turbulence model is used.

## **1.2. Local Scour**

### **1.2.1. Mechanism of scour by turbulent jet**

In general, localised scour can occur in two ways:

- clearwater scour
  
- livebed scour.

Clear water scour happens when the bed material is not in movement. The sediment transported into the contracted section is namely zero. Clear-water scour occurs when the shear stress induced by the water flow passes the critical shear stress of the bed material. Commonly, with clear-water scour, no refilling occurs during the recession of the flood because of lack of sediment supply. Live-bed scour, otherwise, occurs when there is general bed load transport by the stream. Sediment is continually being provided to the areas subjected to scour.

When the diffused jet begins to flow over the primarily smooth moving bed, the pitting potential of the water cannons, generated by the jet flow, is ordinarily very powerful that the sands are directly fenced out from the face and moved downstream at a quick rate. For a short while, the perpendicular extent of the pitrise at a significantly faster than the ground plane and the sand grain is moved as a matter of fact like bed loads. As the scouring zone more and more spread out by passage of time, at the same time the water depth elevated. Out of the basis of continuity, the extending cross sectional area would needed a decrease in the average flow rate. In respect of the local velocity close the bed profile diminishes as the depth of the scouring zone raises. Therefore, the ratio of scouring decreases as time processes. For a longer period, the bed velocity finally reduces to a specific “critical” value as the flow occurs deficiency of removing farther bed material from the scouring zone. At this situation, it could be thought that the scour profile has achieved its “equilibrium” or “asymptotic” state. Indirectly, this proffers that the local bed velocity is directly depends on the notion of a sill of a definite movement.



## **1.2.2. Local scour beneath horizontal jets**

### **1.2.2.1 Scouring Process**

At the beginning of the scouring, downriver of a hydraulic construction (under the water jet) in the event of without apron or an apron when the floor shear stress induced by the horizontal jet passes the critical floor shear stress for the initiation of bed particle motion. The scouring process downstream of a hydraulic structure is complex in nature because of the sudden change of the flow characteristics over the erodible bed and the complex nature of the turbulent jet itself. Different cases of local scour caused by horizontal jets are depicted in Figure 1.1(a) – 1.1(d). Figure 1.1(a) shows a schematic diagram of a typical scour hole developed because of the submerged horizontal jet issuing from a sluice opening downstream of an apron (Hassan and Narayanan, 1985), whereas Figure 1.1(b) depicts a typical scour hole improved because of a submerged horizontal jet issuing from a penstock opening (without apron) directly on the erodible bed (Rajaratnam, 1981a). Also, Figure 1.1(c) shows a diagrammatic scour hole downstream of a spillway apron (Dargahi, 2003) In addition, Figure 1.1(d) presents a scour hole developed due to the flow simultaneously over and under a sluice gate (Uyumaz, 1988).

### **1.2.2.2 Effect of the jet entering a movable bed**

In multiphase model suitable description of the starting circumstance is crucial. These circumstances contain primary grid generations, subsisting phases in space, phase's characteristic and the volume fraction factor of every cell. As soon as these data are supplied the model sets the interphase permutation coefficient, raising force, imaginary mass enforce and interaction force in the middle of the phases and solves the permanence and momentum equations for every phase. The definition the lately occupied volume by every phase, the volume fraction of each phase is calculated by continuity equation. Therefore at the last of every stage, the level of all phase is calculated. This situation goes on as long as the computational progress are converged or a given time period is reached.

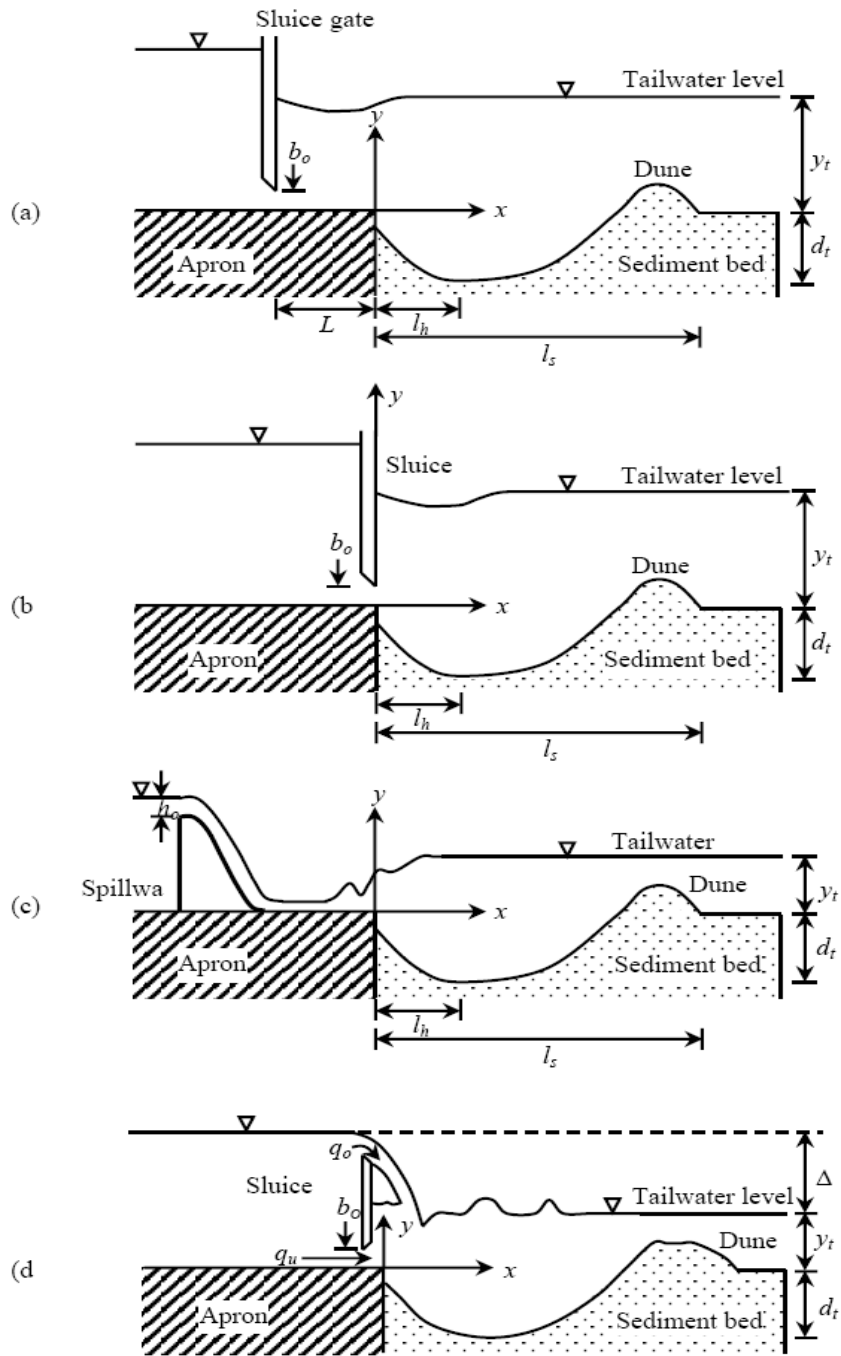


Figure 1.1 Local scour: (a) downstream of an apron after Hassan and Narayanan (1985), (b) due to a submerged horizontal jet without apron (Rajaratnam, 1981a), (c) downstream of a spillway apron (Dargahi, 2003) and (d) due to simultaneous flow over and under a sluice gate after Uyumaz (1988) (Sarkar and Dey 2004).

### **1.2.3 Result of scour hole forming**

Downstream of jet area is reattachment zone in which velocity centreline touching the bottom and makes the scour zone formations. This zone develops increasingly, and its depth gets up. Later the jet reached the bottom and a scour zone is shaped, the velocity centreline divides from the floor, shifts towards the free surface and moves the particle which is then deposits downstream of scour zone.

## CHAPTER 2

### LITERATURE SURVEY

#### 2.1. Applications of RNG k- $\epsilon$ model

The first two equation models for estimating the behaviour of turbulent flows were suggested in 1942 by A.N. Kolmogorow and used the variables  $k$  for fluctuation energy and  $\omega$  for frequency (Kolmogorow, 1942). In 1968, Harlow and Nakayama described k- $\epsilon$  model for turbulence. The second of two previously proposed turbulence transport equations were obtained by Harlow and Nakayama's study so as to determine the variation of several of the universal functions (Harlow and Nakayama, 1968). The re-normalized group (RNG) k- $\epsilon$  turbulence model was first introduced by Yakhot and Orszag (1986).

Karim and Ali (2000) developed a testing procedure for researching the suitability of the FLUENT CFD package in simulating flow models, generated by a turbulent, water jet colliding on rigid horizontal and scoured beds. The scoured beds were recorded at various times of the scouring process. Results derived from using the turbulence models included in FLUENT were examined. After the scouring action had started, the bed shear stress fell and as the scour hole developed further the reduction became less apparent. Usually, flow fields, velocities and shear stresses predicted by FLUENT showed close agreement with relevant experimental results. The results derived from using the RNG k- $\epsilon$  model were virtually identical to those produced by the k- $\epsilon$  model.

A mathematical model was performed by Lu et al (2005). They were simulated the mobile boundaries problem of regional scour round submersible piping. The numeric pattern was shaped of a Renormalized Group turbulence model. Envisaged two cases to confirm the proposed numerical models and the numerical outcomes have shown a positive match to the experimental data. It has been proven that the RNG model is capable of predicting the equilibrium profile of local scour round submersible piping.

Bung et al. (2008) evaluated an experimental study on the flow patterns around a

submerged plate under a propagating bore. Swirls and magnitude of velocity were identified by the Particle Image Velocimetry (PIV) method. Parameters were calculated by the open source code Mat-PIV and verified by numerical simulations via FLOW-3D with the classical  $k-\epsilon$  and the RNG turbulence model. Numerical calculations were performed with use of different turbulence models. Generally, velocity magnitudes were computed with enough precision by all models. But, swirl formation was expressed in differing sensitive. Vortices which have direct simulation by Large Eddy Simulation (LES) method yielded to preferable outcomes describing the processes in more detail.

## **2.2. RANS $k-\epsilon$ model**

Fard, Bakhtiary and Cheng (2005) studied two-phase flow model for simulating early stages of local scour due to steady current under offshore pipelines. Fluid phase was calculated with solving Reynolds Averaged Navier-Stokes (RANS) equations in together with a standard  $k-\epsilon$  turbulence model for turbulence closure using Finite Volume Method in a Cartesian coordinate system. Numerical experiments were showed that inter particle collisions of moving sand grains encourage a predominant micro-mechanism on different stages of local scour around offshore pipelines. The model estimated improvement of scour profiles reasonably well at early stages of onset and jet scour. Failure of the model was estimated an accurate time developments of local scour profiles development through different steps of scour, since one-way calculation was conducted.

Cassan and Belaud (2011) explored the flow field under submerged gates in order to verify frequently used hypothesis about shrinkage coefficient and energy losses. Furthermore it was based on experimental results acquired in a laboratory flume. The flow field was identified experimentally by ADV (Acoustic Doppler Velocimeter) and numerically with RANS (Reynolds Averaged Navier Stokes) simulations conducted with FLUENT software for different configurations of submerged gates and different modeling assumptions. The experimental results on velocity were steady with RANS simulations as far as discharge coefficients, wall shear stress and flow field were concerned. The result of model application showed

that shrinkage coefficients should not be considered as constant at large submergence and large opening, which was a reason of the poor performance of the discharge formulas in these regimes.

Castillo and Carrillo (2008) investigated the energy dissipation in plunge pools. It was produced principally by turbulence generation. The Computational Fluid Dynamics (CFD) model was performed, and it was based on numerical solution of the Navier - Stokes and Reynolds-averaged equations. The laboratory results were permitted calibrating and validating some trading software CFD. As seen, progress was being made in the characterization of the event of turbulent jets with ANSYS-CFX.

### **2.3. Other Models**

Numerical simulation of local scour in front of a vertical wall breakwater was carried by Chen (2006). At this work, Chen developed a two-dimensional numerical wave flume based on Navier-Stokes equations for incompressible and viscous fluid, after he discretized his model by finite element method. Nonlinear waves were created numerically and the standing waves were generated in front of a vertical-wall breakwater. The transports of sediment bed load were modeled to simulate the local scour process at the toe of the breakwater. At his work Chen didn't include a turbulence model. As a result the scouring patterns he obtained good agreement with the results of the earlier work made by Xie (1983).

Hogg and Pritchard (2004) modeled the transport of suspended sediment by a single turbulence event on a sloping breakwater and examined the effects of overtopping on the motion and the redistribution of particles. By increasing use of a Lagrangian frame of reference, the model calculated the net transport by these flows. The results showed that overtopping encouraged the landwards transport of sediment, primarily because the backwash of the swash is significantly weakened. Also the model was quantified the flux of sediment that was transported over the crest to be deposited behind the breakwater.

Adduce (2004) investigated, both experimentally and theoretically, the local scour downstream of turbulent jets due to a sill followed by a rigid apron. The experiments were carried out in a 1 m high, 17 m long and 0.8 m wide sloping flume

of rectangular cross section. Scouring tests were conducted in a 0.8 m wide, 0.3 m high and  $L=3$  m long sediment indentation section, positioned 7 m downstream of the flume inlet by raising artificially the flume bed. For a mobile bed,  $d_{50}= 0.72$  mm sand was used. The flume was equipped with an electromagnetic flow meter, a downstream control gate, positioned at the end of the flume was used to change the downstream water depth. Velocity measurements were conducted by two acoustic instruments: the Ultrasonic Doppler Velocity Profiler and the MicroADV (Acoustic Doppler Velocimeter).

Guven and Gunal (2009) developed a hybrid numerical–mathematical model, which simulated the temporal evolution of local scour and flow patterns in laboratory flumes. The mathematical module calculated the shape of the scour hole by solving an integro-parabolic equation, and the numerical module simulated the two-dimensional laterally averaged flow patterns in the corresponding scour hole. The hybrid model was verified by experimental data taken from the literature. The results proved that the proposed hybrid model could estimate the local scour and flow patterns downstream of a sill followed by a rigid apron, in absolutely good agreement with the experimental results.

In a study by Guney et al. (2011) local scour around bridge piers resulting from unsteady flow were investigated. The experiments were conducted with bimodal sediments in a rectangular flume 18.6 cm long and 80 m wide. The unsteady flow was formed by means of various hydrographs. The bridge pier with circular cross section had a diameter of 7.4 cm. Ultrasonic Velocity Profiler (UVP) was used to measure transient variation of scour depth indirectly. The final depths and configurations of the scours were interpreted in the light of available knowledge.

Azhari et al. (2010) developed a three dimensional numerical model and a physical model to simulate and estimate the local scour depth around a set of three vertical circular piers located in a river. Computations were applied using  $k-\epsilon$  turbulence model. The flow was selected unsteady. The Eulerian granular multiphase model for solving associated equations was applied. Based on the results, the maximum scour depth consisted around the first pier. The time course tests showed that 80% of scour hole is issued in the first hour. The results from the CFD tests showed a good agreement with the experimental data collected from the physical model which an indication of the precision of the chosen CFD procedure.

The mechanism of local scour at a breakwater tip was carried by Chang (1977), which was caused by oblique incident waves on a flat cohesion less bed. Model tests were implemented to determine the scour developments with full reflection from a vertical wall. The shapes of scours were found to be geometrically similar as scour progressed. The connections between wave characteristics and the limiting hole dimensions were introduced.

A studied on the modeling of sediment transport around hydraulic structures is presented in Vuik's (2010), master thesis. The purposes of the study were evaluation the performance of the current way of Delft3D modeling of sediment transport around hydraulic structures in three-dimensional flows, and making recommendations on the modeling of sediment transport around hydraulic structures in hydraulic engineering practice.

Abdelaziz et al (2010) investigated a computation module for sediment transport in open channels which was developed and incorporated into the commercial code FLOW-3D. The results of a model application were described to simulate scour development downstream of an apron due to submerged jet. The bed deformation estimations were compared with measurements, for which the results show usually good agreement compared with experimental data. The model was used to study the effect of percolation discharges on the bed deformation in the flume.

Harb and Zenz (2011) studied on overview about the numeric models for river hydraulics in computational fluid dynamics (CFD) and computing tools used in the domain of water executive was given. Because of the fact that the number of numerical models and computing tools are very wide and still growing, the given list is of course not complete. The studies of authors were showed to models had a varying degree of sophistication and responsibility.

Heather and Smith (2004) researched about modeling the flow and scour around an immovable cylinder. The process of scour around a static horizontal cylinder was modeled using the Computational Fluid Dynamics (CFD) model, FLOW-3D. The model were first assessed by performing hydrodynamic comparisons around a cylinder and five static bed development profiles with laboratory data gained by Jensen et al. (1990). Two turbulence models were evaluated, the Large Eddy Simulation (LES) model and the 2-equation  $k-\epsilon$  transport model. The average horizontal velocity estimates were compared well with the data for both of the turbulence models. The impact of the grid size, bed load porosity, and lifting



parameter were accepted. The grid size was found to have a significant impact on the equilibrium time scale and downstream bed profile shape. Scour shape and depth predictions were in logical agreement with the data.

Wu and Wang (2005) developed the governing equations, model closures, empirical functions and numerical methods of sediment transport models, used with National Center for Computational Hydro science and Engineering's models. (NCCHE). The 2-D models were applied to the estimations of flood flows because of transcending of river banks, dam break or levee breach. The one-dimensional model was used in assessment long-period precipitate in creek and canal meshwork, guessing the sum max diurnal loads in a river basin or watershed, examining the effect of groyne from long-period viewpoint, and many other cases. These ones were become the prescience in resolution support systems.

A Large Eddy Simulation study of the turbulent flow around an obstacle, archetypal of a bridge abutment was presented by Teruzzi et al (2006), with aim to developing on the local scour phenomenon. The turbulent flow characteristics were evaluated through the agency of Large Eddy Simulation, acquiring results both on the averaged flow characteristics as on the sudden ones. The normal and shear stress distributions on the bottom-wall were conducted in comparison with empirical observations relative to erosion phenomena. Data from numerical simulations were allowed a detailed definition of the turbulent flow field and emphasizes in the near obstacle region. The harmony of their results with investigations from flume experiments gives data to the hypothesis that the studied flow field is representative of the phenomenon in spite of the wall boundary condition on the upper surface.

## CHAPTER 3

### NUMERICAL MODEL AND GOVERNING EQUATIONS

#### 3.1. Turbulence model

Turbulent actions are characterized by disordered 3-d vorticity fluctuations. Osborne Reynolds (1842-1912) was one of the first investigators who defined this phenomenon. Reynolds concluded that the formation of turbulence is related on the ratio between inertial forces and viscous forces. The dimensionless Reynolds number is based on this ratio:

$$Re = \frac{UL}{\nu} = \frac{\rho UL}{\mu} \quad (1)$$

Where  $U$  denotes a characteristic velocity difference [m/s] and  $L$  is a length scale [m], respectively, and  $\nu$  is the kinematic viscosity [ $m^2/s$ ], a fluid property related to the dynamic viscosity  $\mu$  by  $\nu = \mu/\rho$ . In this expression turbulent flows are defined as flow with approximately  $Re > 4000$ . Flow with  $Re < 2100$  is called laminar flow. The zone in between is called the transition zone. In Civil Engineering application, almost all flows are turbulent flows, since  $Re \gg 10^5$ .

#### 3.2. The k- $\epsilon$ Turbulence Model

The k-epsilon model is the very important alternative. It has a two equation model, which means that it contains two additional carriage equations to display the turbulent properties of the flow.

The base hypothesis of this method is that the local state of turbulence is characterized by the two parameters  $k$  and  $\epsilon$ , which are corresponding to the parameter pair  $k$  and  $L$  because  $\epsilon$  is proportional to  $k^{3/2}/L$ . The one of the most

significant facility that the k-ε model supplies is that the energy dissipation, ε, is included in kinetic energy equation and does not require an extra source term.

The k-ε turbulence model investigated by Harlow and Nakayama in 1968 is still widely used two equation eddy viscosity turbulence.

There are three types of k-ε turbulence models.

- Standard k-ε turbulence models
- RNG (renormalize) k-ε turbulence models
- Realizable k-ε turbulence models

### 3.2.1. Standard k-ε Turbulence Model

In eddy viscosity turbulence models like k – ε model the Reynolds stresses are dependent to the velocity gradients over the turbulent viscosity, this correlation is named the Boussinesq supposition, where the Reynolds stress tensor in the time averaged Navier-Stokes equation is regenerated by the turbulent viscosity multiplied by the velocity gradients. This can be showed as (Boussinesq, 1877);

$$-\overline{\rho u_i u_j} = \rho \nu_t \left( \frac{\partial U_i}{\partial x_j} + \frac{\partial U_j}{\partial x_i} \right) - 2/3 k \delta_{ij} \quad (2)$$

For Reynolds stresses, where  $\nu_t$  is determined from dimensional analysis of k and ε. In this equation,  $U_i$  denotes the mean velocity component, and  $x_i$  is the space coordinate. The distributions of k and ε are determined from equation (3-4).

For turbulent kinetic energy k;

$$\frac{\partial}{\partial t} (\rho k) + \frac{\partial}{\partial x_i} (\rho k u_i) = \frac{\partial}{\partial x_j} \left[ \left( \mu + \frac{\mu_t}{\sigma_k} \right) \frac{\partial k}{\partial x_j} \right] + P_k + P_b - \rho \epsilon - Y_M + S_k \quad (3)$$

For dissipation ε;

$$\frac{\partial}{\partial t} (\rho \epsilon) + \frac{\partial}{\partial x_i} (\rho \epsilon u_i) = \frac{\partial}{\partial x_j} \left[ \left( \mu + \frac{\mu_t}{\sigma_\epsilon} \right) \frac{\partial \epsilon}{\partial x_j} \right] + C_{1\epsilon} \frac{\epsilon}{k} (P_k + C_{3\epsilon} P_b) - C_{2\epsilon} \rho \frac{\epsilon^2}{k} + S_\epsilon \quad (4)$$

The turbulent viscosity (called eddy viscosity),  $\mu_t$ , is calculated by combination of  $k$  and  $\varepsilon$  equations:

$$\mu_t = \rho C_\mu \frac{k^2}{\varepsilon} \quad (5)$$

The terms  $C_k$ ,  $C_\varepsilon$ ,  $C_{1\varepsilon}$ ,  $C_{2\varepsilon}$  and  $C_{3\varepsilon}$ , are called the turbulence model coefficients. The symbol of the  $P_k$  is the production rate of turbulence,  $P_b$  is the production rate of turbulence due to buoyancy,  $Y_M$  demonstrate the addition of the undulating dilatation in compressible turbulence to the overall dissipation rate. The model constants  $C_{1\varepsilon}$ ,  $C_{2\varepsilon}$ ,  $C_\mu$ ,  $\sigma_k$  and  $\sigma_\varepsilon$  have the following default values:

$$C_{1\varepsilon} = 1.44, C_{2\varepsilon} = 1.92, C_\mu = 0.09, \sigma_k = 1.0, \sigma_\varepsilon = 1.3 \quad (6)$$

The application of the k- $\varepsilon$  method in modeling flow turbulence can be widely seen in many different areas of science as: mechanical, aeronautical engineering and many subjects in hydraulic engineering has been found to work well with the standard constants in many cases. But it has also been determined that the model does not work very well for some complex flows such as separated flows and flows in curved geometries. (Versteeg and Malalasekera 1995, Wilcox 1998).

The main weakness of the model is that it overestimates the turbulence. And also the model has a tendency to under-predict the size of separation regions in unconfined flow (e.g. behind bluff bodies), but various modifications to the  $\varepsilon$ -equation have been suggested to improve the performance, and to eliminate the weaknesses but none of these modifications work entirely satisfactory. (Rodi 1980, Launder and Spalding 1974). For example; Hanjalic and Launder tried to make the production of  $\varepsilon$  more sensitive to normal stress than to shear stress (Hanjalic and Launder 1972).

### 3.2.2. RNG k- $\varepsilon$ Turbulence Model

The RNG model was first announced by Yakhot and Orszag (1986). In this model, the Navier-Stokes equations are renormalized to simulate the effects of smaller scales of motion. The RNG turbulence model does analysis for  $k$  and  $\varepsilon$ . The RNG model applies statistical ways for a derivation of the averaged equations for turbulent quantities, such as  $k$  and  $\varepsilon$ . This model is appeared from the exact Navier-Stokes

equations, using a mathematical technics called “Re-Normalization Group”. The RNG model utilizes equations similar to the equations for the Standard k-ε model. In addition, in RNG model the specification of turbulence characteristic feature as  $k$  and  $\varepsilon$  is ensured by use of statistical methods.

The RNG  $k - \varepsilon$  model has known benefits when there is strong curvature in the streamlines, as is the case with the accelerating flow over the weir. The standard  $k-\varepsilon$  model is known to be of limited correctness when used to model flow over rocky bodies such as the weir. Normally, this model is widely used than the standard  $k-\varepsilon$  model.

The RNG  $k - \varepsilon$  model has a same mode to the standard  $k-\varepsilon$  model:

$$\frac{\partial}{\partial t}(\rho k) + \frac{\partial}{\partial x_i}(\rho k u_i) = \frac{\partial}{\partial x_j} \left[ \left( \alpha_k \mu_{eff} \frac{\partial k}{\partial x_j} \right) \right] + P_k + P_b - \rho \varepsilon - Y_M + S_k \quad (7)$$

and

$$\frac{\partial}{\partial t}(\rho \varepsilon) + \frac{\partial}{\partial x_i}(\rho \varepsilon u_i) = \frac{\partial}{\partial x_j} \left[ \left( \alpha_\varepsilon \mu_{eff} \frac{\partial \varepsilon}{\partial x_j} \right) \right] + C_{1\varepsilon} \frac{\varepsilon}{k} (P_k + C_{3\varepsilon} P_b) - C_{2\varepsilon} \rho \frac{\varepsilon^2}{k} - R_\varepsilon + S_\varepsilon \quad (8)$$

$$P_k = -\rho \overline{u_i u_j} \frac{\partial u_j}{\partial x_i} \quad (9)$$

To appraise  $P_k$  in a stable manner with the Boussinesq hypothesis,

$$P_k = \mu_t S^2 \quad (10)$$

In this equation,  $S$  is the module of the average rate of strain tensor, described as

$$S \equiv \sqrt{2S_{ij}S_{ij}} \quad (11)$$

$P_b$  is given by

$$P_b = \beta g_i \frac{\mu_t}{Pr_t} \frac{\partial T}{\partial x_i} \quad (12)$$

The Turbulent Prandtl number  $Pr_t$  is the ratio of the fluid viscosity to the thermal conductivity of a substance.  $Pr_t$  is 0.85 for standard and realizable  $k - \varepsilon$  models. For RNG  $k-\varepsilon$  model,  $Pr_t = 1/a$ . The opposite efficient Prandtl numbers,  $\alpha_k$  and  $\alpha_\varepsilon$ , are calculated using this formula:

$$\left| \frac{\alpha - 1.3929}{a_0 - 1.3929} \right|^{0.6321} \left| \frac{\alpha + 2.3929}{a_0 + 2.3929} \right|^{0.3679} = \frac{\mu_{mol}}{\mu_{eff}} \quad (13)$$

In this equation,  $a_0=1$  in the high Reynolds number limit ( $\mu_{mol}/\mu_{eff} \ll 1$ ),  $a_k = a_\varepsilon \approx 1.393$  the parameter of thermal dilatation,  $\beta$ , is described as

$$\beta = -\frac{1}{\rho} \left( \frac{\partial \rho}{\partial T} \right) \quad (14)$$

The scale elimination procedure in RNG theory results in a differential equation for turbulent viscosity:

$$d\left(\frac{\rho^2 k}{\sqrt{\varepsilon\mu}}\right) = 1.72 \frac{\dot{v}}{\sqrt{\dot{v}^3 - 1 + C_v}} d\dot{v} \quad (15)$$

where

$$\begin{aligned} \dot{v} &= \mu_{eff}/\mu \\ C_v &\approx 100 \end{aligned} \quad (16)$$

Eq. (15) is embedded to achieve an exact definition of how the efficient turbulent carriage varies with the efficient Reynolds number, permitting the pattern to preferable process low Reynolds issue and close the wall flux. In the high Reynolds number limit, this equation gives

$$\mu_t = \rho C_\mu \frac{k^2}{\varepsilon} \quad (17)$$

With  $C_p = 0.0845$  obtained using RNG theory. In standard  $k$ - $\varepsilon$  model this value is 0.09.

Generally turbulence is affected by swirl or rotation in the average flow. The RNG model allows an alternative to calculation for the impacts of vortex or spins by alteration the turbulent viscosity properly. The alteration gets the subsequent useful shape eq. (18).

$$\mu_t = \mu_{t0} f\left(\alpha_s, \Omega, \frac{k}{\varepsilon}\right) \quad (18)$$

In there,  $\mu_{t0}$  is the rate of turbulent viscosity computed besides the vortex alteration using either eq. (19) or eq. (20).

$$d\left(\frac{\rho^2 k}{\sqrt{\varepsilon\mu}}\right) = 1.72 \frac{\dot{v}}{\sqrt{\dot{v}^3 - 1 + C_v}} d\dot{v} \quad (19)$$

$$\mu_t = \rho C_p \frac{k^2}{\varepsilon} \quad (20)$$

$\Omega$  is a called typical vortex number.  $\alpha_s$  denotes a vortex constant that supposed varied rates depending on if the flow is swirl dominated or only mildly swirling. For moderately swirling flows,  $\alpha_s$  is set to 0.05. For violently swirling flows, a greater than worth of  $\alpha_s$  can be used.

The most important distinction among the RNG and standard  $k$  -  $\varepsilon$  models lies in the supplementary term in the  $\varepsilon$  equation given by

$$R = \frac{C_p \rho \eta^3 (1 - \eta/\eta_0) \varepsilon^2}{1 + \beta \eta^3} \frac{1}{k}$$

Where  $\eta \equiv Sk/\varepsilon$   $\eta_0 = 4.38$   $\beta = 0.012$  (22)

Then  $\varepsilon$  equation is given by this formula;

$$\frac{\partial}{\partial t}(\rho\varepsilon) + \frac{\partial}{\partial x_i}(\rho\varepsilon u_i) = \frac{\partial}{\partial x_j} \left( \alpha_\varepsilon \mu_{eff} \frac{\partial \varepsilon}{\partial x_j} \right) + C_{1\varepsilon} \frac{\varepsilon}{k} (P_k + C_{3\varepsilon} P_b) - C_{2\varepsilon} \rho \frac{\varepsilon^2}{k} - R_\varepsilon + S_\varepsilon \quad (23)$$

Using Equation

$$R = \frac{C_p \rho \eta^3 (1 - \eta/\eta_0) \varepsilon^2}{1 + \beta \eta^3} \frac{1}{k} \quad (24)$$

In  $\varepsilon$  formulation, last two locutions can be combined, and the result of formula can be rewritten as

$$\frac{\partial}{\partial t}(\rho\varepsilon) + \frac{\partial}{\partial x_i}(\rho\varepsilon u_i) = \frac{d}{dx_j} \left( \alpha_\varepsilon \mu_{eff} \frac{\partial \varepsilon}{\partial x_j} \right) + C_{1\varepsilon} \frac{\varepsilon}{k} (P_k + C_{3\varepsilon} P_b) - C_{2\varepsilon}^* \rho \frac{\varepsilon^2}{k} \quad (25)$$

In this equation  $C_{2\varepsilon}^*$  is given by

$$C_{2\varepsilon}^* \equiv C_{2\varepsilon} + \frac{C_p \eta^3 (1 - \eta/\eta_0)}{1 + \beta \eta^3} \quad (26)$$

The model constants  $C_{1\varepsilon}$  and  $C_{2\varepsilon}$  are

$$C_{1\varepsilon} = 1.42 \quad C_{2\varepsilon} = 1.68 \quad (27)$$

Consequently, in jet flows, the RNG model efficiency a lower turbulent viscosity than the standard  $k - \varepsilon$  model. For this reasons, the RNG model is more compatible to the effects of rapid strain and streamline curvature than the standard  $k - \varepsilon$  model, which describes the excellent performance of the RNG model for specific classes of flows.

### 3.2.3. Realizable k-ε Turbulence Model

This model contains a new transport equation for the turbulent dissipation rate  $\varepsilon$ . Also, a critical coefficient of the model,  $C_\mu$ , is expressed as a function of mean flow and turbulence properties, rather than assumed to be constant as in the standard model. This allows the model to satisfy certain mathematical constraints on the normal stresses consistent with the physics of turbulence (realizability). The concept of a variable  $C_\mu$  is also consistent with experimental observations in boundary layers.

Similar to the RNG model, the form of the  $k$  formulation is identical to the one in. But, the shape of the  $\varepsilon$  formulation is fairly varied shape those in the standard and RNG based  $k - \varepsilon$  models. The modelled transport formulation for  $k$  and  $\varepsilon$  in the realizable  $k - \varepsilon$  model are

$$\frac{\partial}{\partial t}(\rho k) + \frac{\partial}{\partial x_j}(\rho k u_j) = \frac{\partial}{\partial x_j} \left[ \left( \mu + \frac{\mu_t}{\sigma_k} \right) \frac{dk}{dx_j} \right] + P_k + P_b - \rho \varepsilon - Y_M + S_k \quad (28)$$

and

$$\frac{\partial}{\partial t}(\rho \varepsilon) + \frac{\partial}{\partial x_j}(\rho \varepsilon u_j) = \frac{\partial}{\partial x_j} \left[ \left( \mu + \frac{\mu_t}{\sigma_\varepsilon} \right) \frac{d\varepsilon}{dx_j} \right] + \rho C_1 S_\varepsilon - \rho C_2 \frac{\varepsilon^2}{k + \sqrt{\nu \varepsilon}} + C_{1\varepsilon} \frac{\varepsilon}{k} C_{3\varepsilon} P_b + S_\varepsilon \quad (29)$$

$$\text{where} \quad C_1 = \max \left[ 0.43, \frac{\eta}{\eta + 5} \right], \eta = S \frac{k}{\varepsilon}, \quad S = \sqrt{2 S_{ij} S_{ij}} \quad (30)$$

The constants of model are  $C_{1\varepsilon}$ ,  $C_2$ ,  $\sigma_k$  and  $\sigma_\varepsilon$  have been based to provide that the model builds great for specific standard flows. The model constants are

$$C_{1\varepsilon} = 1.44 \quad C_2 = 1.9 \quad \sigma_k = 1.0 \quad \sigma_\varepsilon = 1.2 \quad (31)$$

This model has been commonly verified for a various flows including rotating homogeneous shear flows, free flows jets and mixing layers, canal and border layer flows, and divided flows. For all these situations, the achievement of the pattern was determined to be significantly better than standard  $k-\varepsilon$  model.



## CHAPTER 4

### DESCRIPTION OF THE EXPERIMENTAL AND THE NUMERICAL MODELS

#### 4.1 Description of the Experimental Model

In this study, no experimental work has been carried out. The experimental results recorded by Adduce (2004) was used in calibration and validation of the proposed numerical model.

Two dimensional scour profiles are investigated by Adduce (2004)'s experiments. The experimental setup was designed in a 17 m long flume with rectangular cross section of 0.8 m width and 1 m height. The experimental model includes 0.8 m width, 0.3 m height and 3 m length scouring test section and it was filled with sand. The density of the sand was  $\rho_s=2650 \text{ kg/m}^3$  and porosity  $p=0.44$  used in the tests. An erodible bed  $d_{50}=0.72 \text{ mm}$ ,  $d_{90}=0.96 \text{ mm}$  was followed by a sill with height  $z=0.15 \text{ m}$  and length  $L_p=0.5 \text{ m}$ , which was mounted upstream of the experimental model.

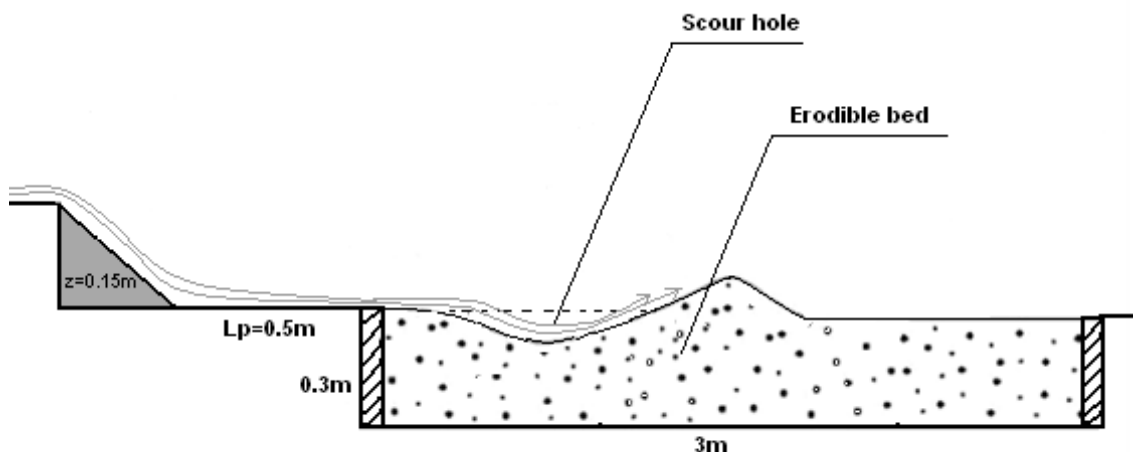


Figure 4.1 Schematic drawing of scouring caused by jet

To change the downstream of water height, a control gate was used. It was placed at the end of the canal. The water levels in the canal were measured with a point measure of precision = 0.10 mm was placed on a transporter, which moved

through channel. At the entrance of the water discharge was measured with an electromagnetic flow-meter and controlled by an inlet valve. The movement of the sand bed was blocked by increasing the water evacuation slowly and adjusting to the intended experimental rate.

The water evacuation ( $Q$ ) was kept constant for the throughout the experimental period. To record the development of the scour, charge-coupled device camera was used. Velocity measurements applied by an UDV at the end of the experiment. The experimental conditions are showed in Table 4.1. In addition to this, in Table 4.1 the inlet velocity entering the mobile bed section ( $U_1$ ), a maximum depth of scour ( $S_{max}$ ), a maximum length of scour ( $L_s$ ), and the test duration ( $T$ ) for each test are also reported. The data obtained Adduce (2004) is given in Table 4.1.

Table 4.1 Experimental conditions used in model validation (Adduce, 2004)

Test	$Q$ (m <sup>3</sup> /s)	$U_1$ (m/s)	$h_s$ (m)	$y_t$ (m)	$S_{max}$ (m)	$L_s$ (m)	$T$ (min)
<b>t1</b>	0.0123	3.074	0.023	0.129	0.044	0.375	580
<b>t2</b>	0.0162	3.089	0.026	0.137	0.061	0.600	480
<b>t3</b>	0.0184	3.072	0.028	0.143	0.067	0.630	580
<b>t4</b>	0.0263	3.146	0.033	0.156	0.082	0.800	450

## 4.2 The Numerical Model

Computational Fluid Dynamics is an important supply to recreate events such as wave run-up and thus aids in understanding the underlying factors causing it. As the growing use of CFD in engineering analysis is pronounced it is important to make sure that the results from the simulation are in tandem with the theoretical and published results.

The CFD calculations shown here are based on simulated solutions to the Re-Normalisation Group (RNG) k- $\epsilon$  equations, carried out using FLUENT software. The prediction of the scour profile in the package is based on the Eulerian three-phase model. It is successfully validated to be suitable for modelling granular flows which in the scope of this thesis.

In this study FLUENT software is while developing the numerical model of both

the temporal moving bed and the hydrodynamic flow characteristics. GAMBIT software is used to construct the solution domain geometry and the meshing of the faces. Then, the generated grid including the boundary conditions is transferred to Fluent's solver. These steps are explained in following sections in detail.

#### **4.2.1. Solution Method (GAMBIT and FLUENT)**

##### **4.2.1.1. GAMBIT**

Gambit is a common-purpose pre-processor for CFD analysis of Fluent, it continuing to allow engineers; easier access into the CFD world. Gambit's features set new industry standards in meshing software. GAMBIT is the short form for: Geometry and Mesh Building Intelligent Toolkit.

Gambit can be used for:

- Geometry construction
- Mesh generation for all Fluent solvers
- Mesh quality examination
- Boundary zone assignment

The general operation sequence for Gambit is as follows

- Initial setup
- Geometry Creation
- Meshing
- Mesh examination
- Zone assignment
- Mesh export

The main policy for creating geometry using Gambit is to start from the lowest topology and go to higher topologies:

- *Vertexes* are basic points that we use to describe our geometry or domain. These points must be entered by using the x-y-z coordinate system. Figure 4.2 shows the defining vertex.

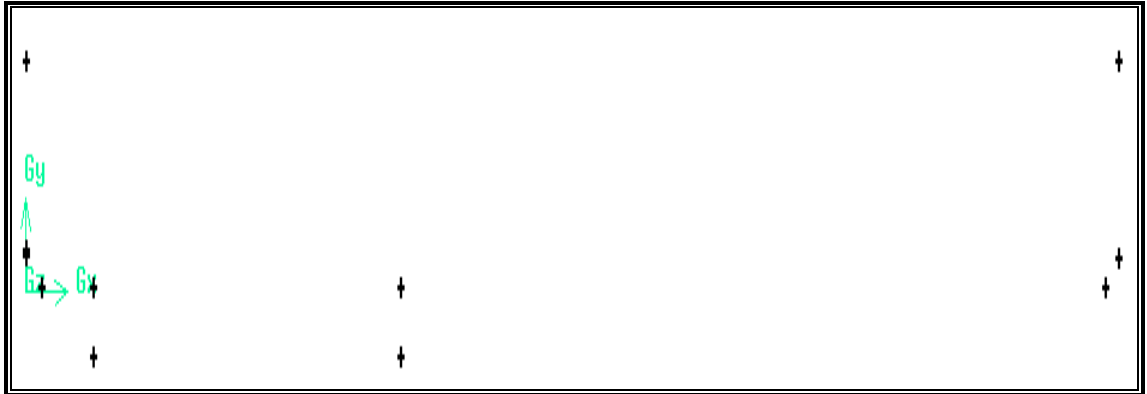


Figure 4.2 Defining vertexes using GAMBIT

- We'll now connect appropriate pairs of vertices to form edges (Figure 4.3). *Edges* are lines that we create by combining the vertices of the lower topology. To select any entity in GAMBIT, hold down the SHIFT key and click on the entity.

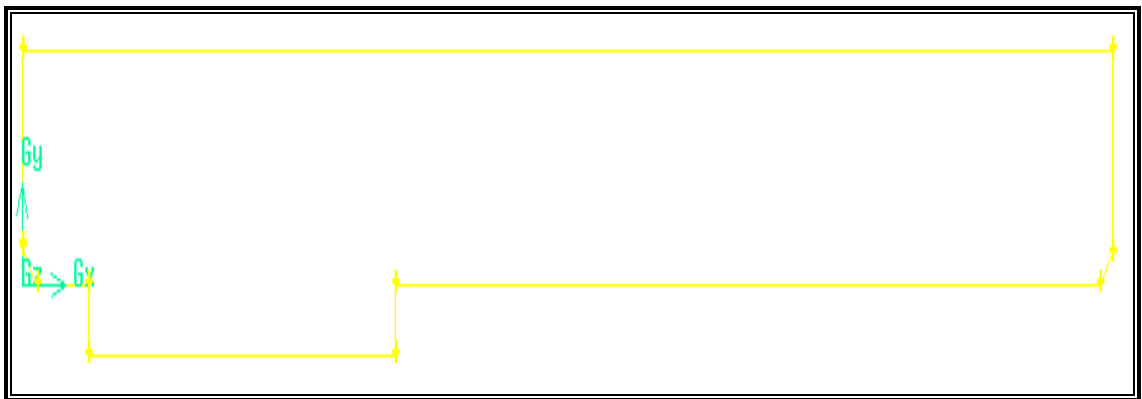


Figure 4.3 Defining edges using GAMBIT

- To form a *face* we need a number of lines. We can select suitable edges by SHIFT button and we can create face by using apply button. The selected edges must provide a closed area. Figure 4.4 is simple example that shows faces.

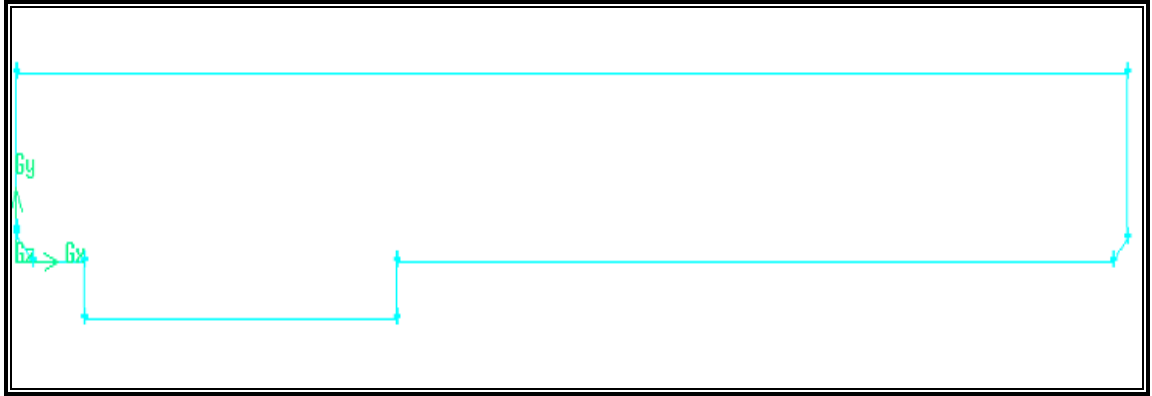


Figure 4.4 Defining faces using GAMBIT

- A *volumes option* is used to create volume by combining faces of lower topology. (for three dimension)

The created faces will be divided into smaller faces called meshes. The spacing of the meshes can be selected. In addition the mesh spacing can be set to be smaller at the areas where the flow is thought to get more sensitive. The spacing of the grids is highly related with the accuracy of the results so one should be careful not to pick the spacing too wide so that results will be coarse or not too small so it will take a long time for computing.

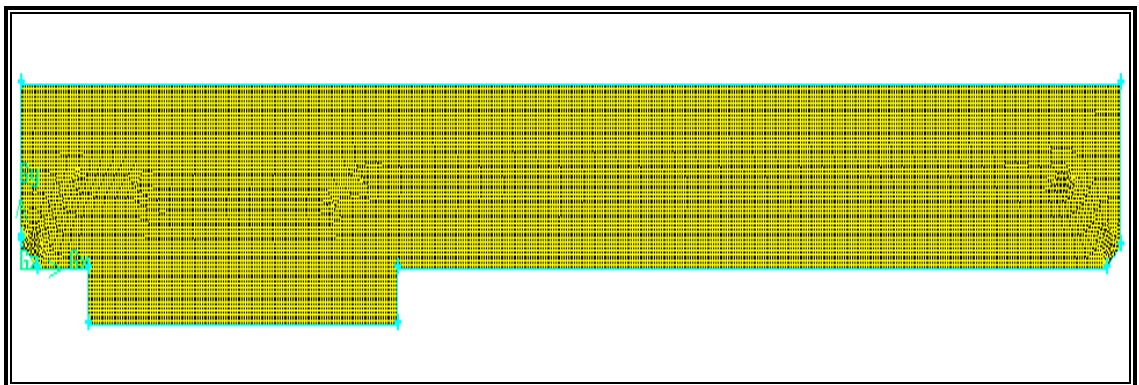


Figure 4.5 Defining meshes using GAMBIT

The geometry was then created using GAMBIT a pre-processor software for FLUENT. The meshed surfaces were composed of 0.025m x 0.025m; 18099 quadrilateral cells. Figure 4.5 and Figure 4.6 displays the drawing of the numerical flume that'll be taken into consideration.

The appropriate boundary conditions can be determined with SHIFT key using the edges. These conditions will be detailed in FLUENT section in this paper. After processing GAMBIT, study will be exported as a mesh file, for a FLUENT.

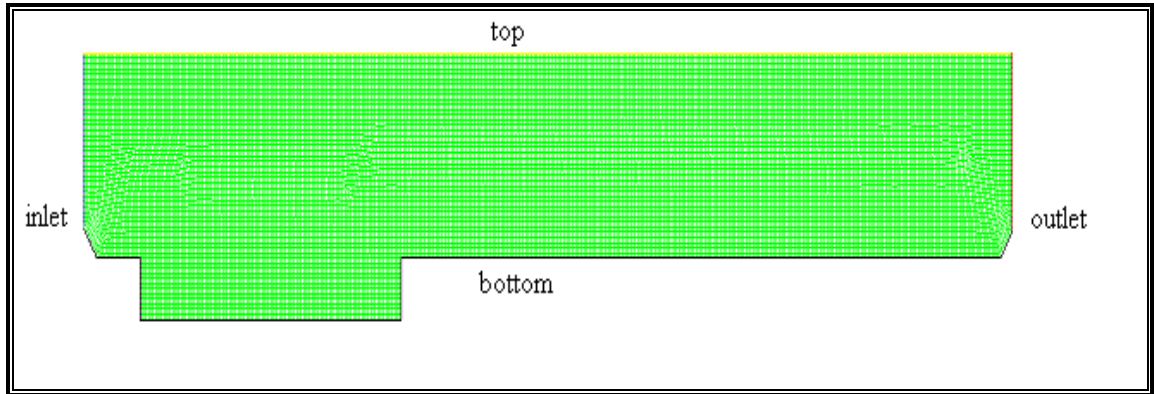


Figure 4.6 Displaying the boundary conditions using GAMBIT

#### 4.2.1.2. FLUENT

FLUENT is a CFD computer program, it used to simulate the fluid flow and heat transfer in complex geometries. It uses the finite volume technique to resolve the governing equations for a liquid. It allows the ability to use varied physical models. Grid generation and image is done using GAMBIT which is the pre-processor together with FLUENT. FLUENT additionally allows you to refine or coarsen your network set on the current resolution. The main steps of the modelling by Fluent software are.

- Problem definition and pre-processing:
  - Specify your modelling purposes
  - Specify the zone of modelling
  - Design and create the grid
- Solving:
  - Design the numeric model
  - Start iterations for solution and observe
- Post-processing:
  - Analyse the outcome data
  - Make adjustments to the model if necessary

## 4.2.2 The numerical modelling steps

The pressure-based, unsteady, implicit solver is applied along with the three phase Euler scheme to simulate the process in two dimensional. According to the pressure-based solvers, velocity field is obtained from the momentum equation, mass conservation (continuity) is achieved by solving a pressure correction equation, energy equation (where appropriate) is solved sequentially, additional scalar equations are solved in a segregated fashion and the PBS can be run implicit only (explicit would be not efficient).

### 4.2.2.1. Turbulence modelling and implementation of the boundary conditions

For forming the Reynolds stresses the RNG k-epsilon model as implemented in Fluent 6.3.26 is used with differential viscosity model for turbulence flows including pressure gradient effects with the proposed constants implemented as default in the program. For the wall modelling the standard wall treatment is selected. The k-ε multiphase model is selected as the mixture.

The primary phase is selected as water, the secondary phase is adapted to be sand and tertiary phase is selected air. Since FLUENT doesn't contain sand as a default material, in its database a new material is formed. The sand particles are consisted a diameter of 0.00072 m and a density of 2650 kg/m<sup>3</sup> as used in Adduce (2004). Granular is ticked under the phases menu to determine the condition of the bed. Drag coefficient is selected based on Symlal-O'Brien methods for sand-water interaction. For air-sand interaction, drag force is neglected. Symlal O'Brien (Symlal and O'Brien, 1989) suggested the drag factor model which is based on evaluation of the extreme velocities of corpuscles in fluidised or settling beds as:

$$K_{sl} = \frac{3a_s a_1 \rho_1}{4v_{r,s}^2 d_s} C_D \left( \frac{Re_s}{v_{r,s}} \right) |\vec{v}_s - \vec{v}_l| \quad (32)$$

where  $Re_s$  is the relative Reynolds number expressed by

$$Re_s = \frac{\rho_l d_s |\vec{v}_s - \vec{v}_l|}{\mu_l} \quad (33)$$

$v_{r,s}$  is the terminal velocity correlation for the solid phase:

$$v_{rs} = 0.5(A - 0.06Re_s + \sqrt{(0.06Re_s)^2 + 0.12Re_s(2B - A) + A^2}) \quad (34)$$

With  $A = a_1^{4.14}$  and  $B = 0.8a_1^{1.28}$  for  $\alpha_1 \leq 0.85$ , and  $B = a_1^{2.65}$  for  $\alpha_1 > 0.85$ .

To apply the gravitational acceleration, Gravity is selected under the operating conditions menu and value is written as a -9.81 with y direction.

The Boundary Conditions panel allows us to set the type of a zone and display other panels to set the boundary condition parameters for each zone. The velocity components, turbulence properties and other scalar properties are prescribed at the inlet boundary. A uniform velocity is applied on the inlet boundary as 3.074 m/s for test1, look at other values from table 1.

Outlet Conditions are used to exits of model flow where the details of the flow velocity and pressure are not known prior to solving the flow problem. Outflow boundaries conditions cannot be define at Fluent GUI. It extrapolates the required information from the interior domain nodes.

Symmetry boundary conditions were elected at the free surface, which enforces a zero normal velocity and a zero shear stress. Use of a symmetry boundary condition in this way is a standard practice for such distant, open boundaries. For a bottom conditions, a no-slip condition is imposed, all flow vertical to the wall is set to zero. The bed roughness factor is calculated using a procedure given by FLUENT (default roughness constant is 0.5). For turbulent flows, roughness conditions can be specified.

### **4.2.3 Time-based solution and the convergence criteria**

The different regions are patched in order to define the areas of phases at the initial stage (Figure 5.5). The area of scour was defined as sand material.

In CFD analysis the numerical model is not only discretized in space, but also in time. In time we always have to make an approximation to the ideal solution. The time step  $\Delta t$  must be small enough to resolve time dependent features and to ensure convergence within the maximum number of iterations set by the user. For this study, time step size was taken as a 0.01 sec and with 15 iterations per time step. Each model was run till the convergence criterion was reached. The default convergence criterion on Fluent solver was used in this study.



## CHAPTER 5

### RESULTS AND DISCUSSION

The calculation of sand profiles require a number of parameters to be monitored, however these are only some of the many variables. Data sets and graphical representations can be extracted both during analysis and post processing. For a full description of the available information, the reader is cited to the FLUENT User Manual (2006). Sand profile elevations are determined at particular instant using inbuilt functions within the software that plots a contour for a particular quantity. To obtain the surface profile plots, the required that is to be extracted for the volume fraction=0.5 which defines the interface between the water phase ( $vf=1$ ) and the sand phase ( $vf=0$ ) at each water-sand interface cell.

In the Figures 5.1-5.4, the experimental results (dots) and FLUENT's predictions of asymptotic profile (black line) for each test are shown, respectively. As a general view from Figures 5.1-5.4, the geometry of the scour hole increases with increasing flow rates. These holes disappear moving downstream along the scour profile.

A considerably good agreement is monitored among the estimated and monitored scoured bed profiles for all tests. But, especially in dune section, Fluent's predictions are far from accuracy. Generally, it can be deduced that Fluent predicted the maximum scour depth to be earlier than the measured one.

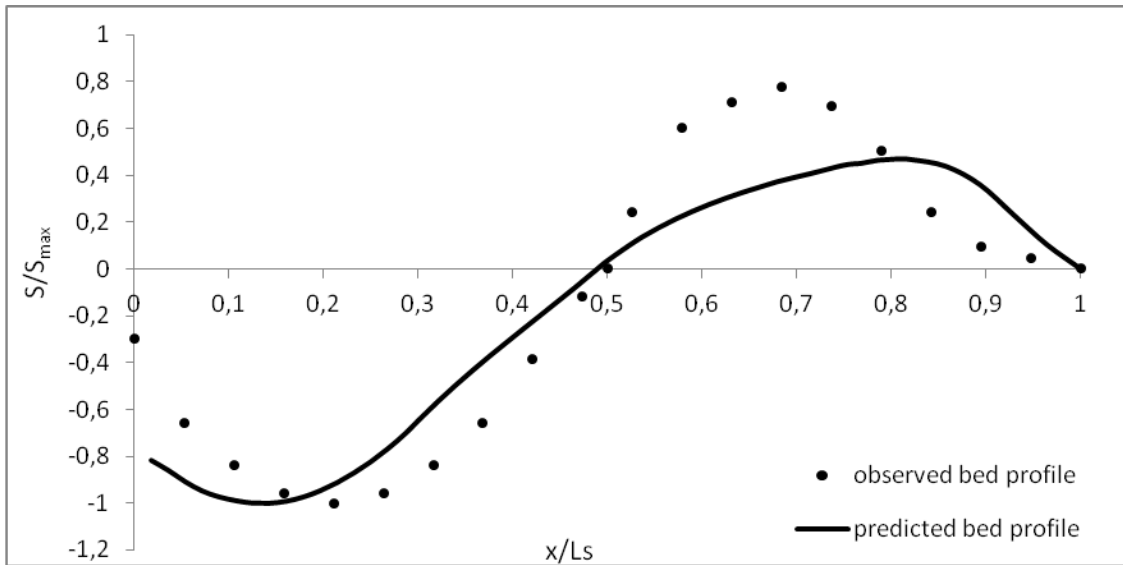


Figure 5.1 Fluent's asymptotic scour profile vs. measured Adduce (2004)'s for test 1.

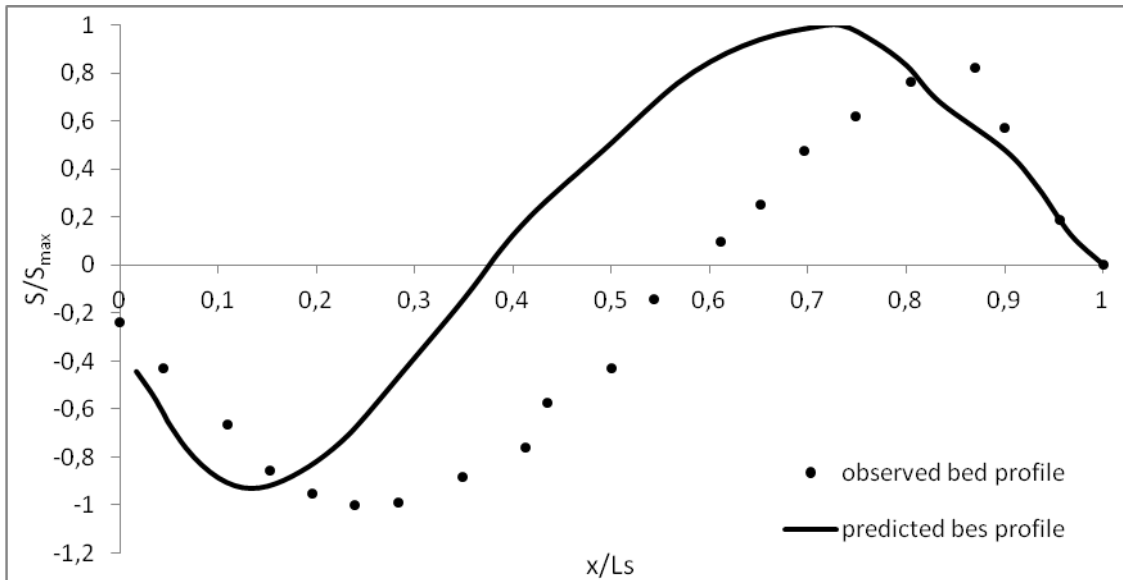


Figure 5.2 Fluent's asymptotic scour profile vs. measured Adduce (2004)'s for test 2.

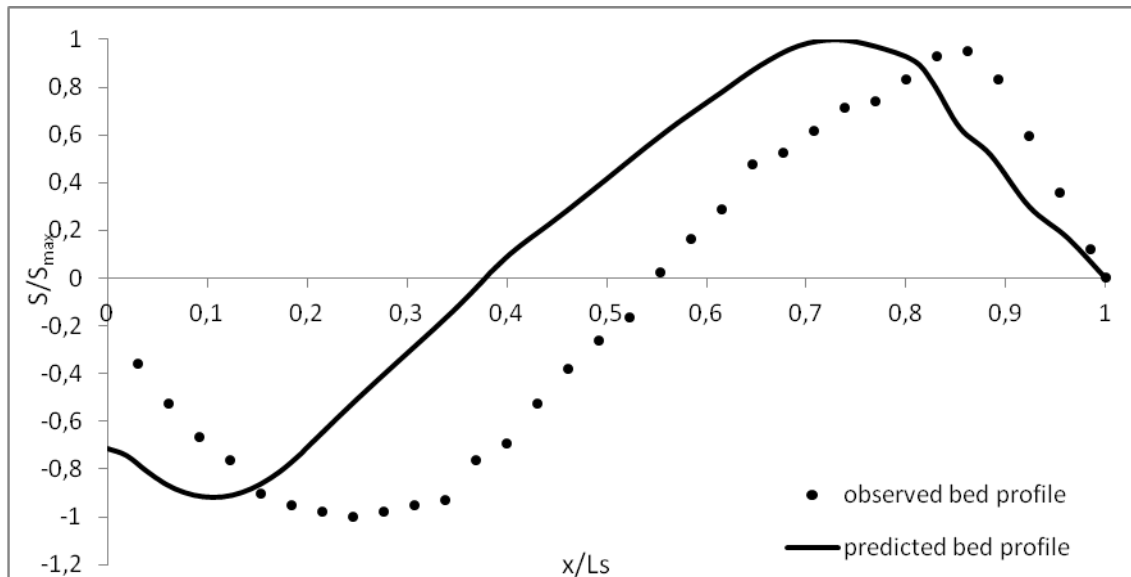


Figure 5.3 Fluent's asymptotic scour profile vs. measured Adduce (2004)'s for test 3.

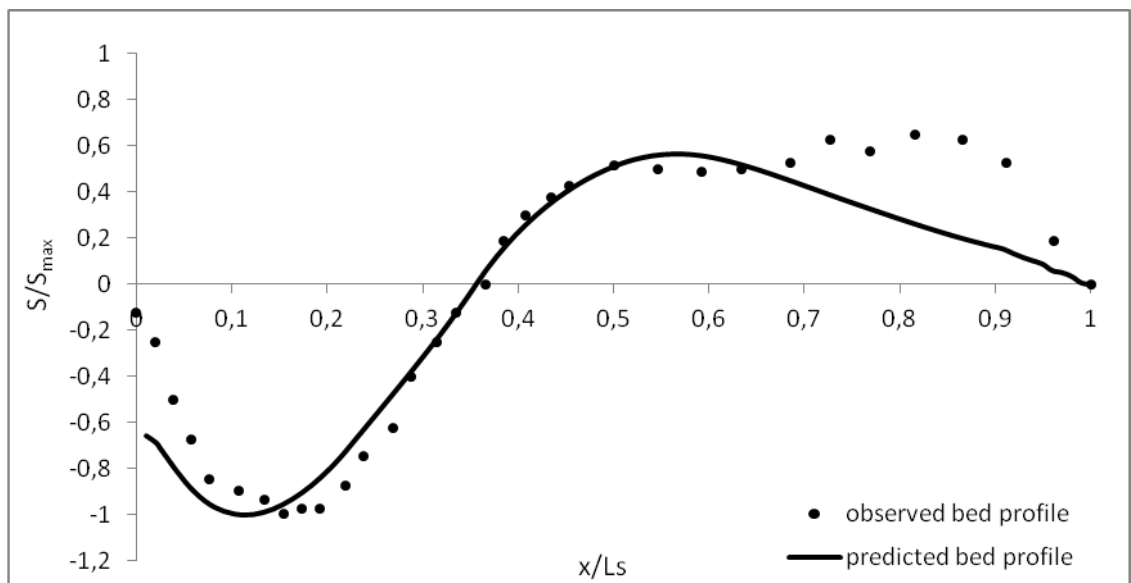


Figure 5.4 Fluent's asymptotic scour profile vs. measured Adduce (2004)'s for test 4.

Under-predictions of the present model can be explained by the idealization of the proposed 3-phase mixture model especially in boundary of each layer. It should be noted that Fluent software is not capable of modelling the temporal change of scouring bed profile, since it does not contain a sediment transport model. The 3-phase mixture model is proposed for this purpose. Moreover, we introduced the sand material manually to the solver of Fluent, since Fluent does not contain sand as a

default material. The drag force effect between each material surface was also introduced manually based on the empirical studies of others.

FLUENT permits the user to plot contour lines or profiles superimposed on the physical domain. Contour lines are lines of constant magnitude for a selected variable (isotherms, isobars, etc.). Figure 5.5 shows a drawing of filled contours of pressure at initial stage for test 1. This figure is valid also for the cases of tests 2-4. Figure 5.6 is an illustration of the contours of volume fractions of water phase for test 1. Figure 5.7 shows the concentration of the deposited materials around the scour hole for test 1. Figures 5.8-5.13 represent the same illustrations for test 2-4.

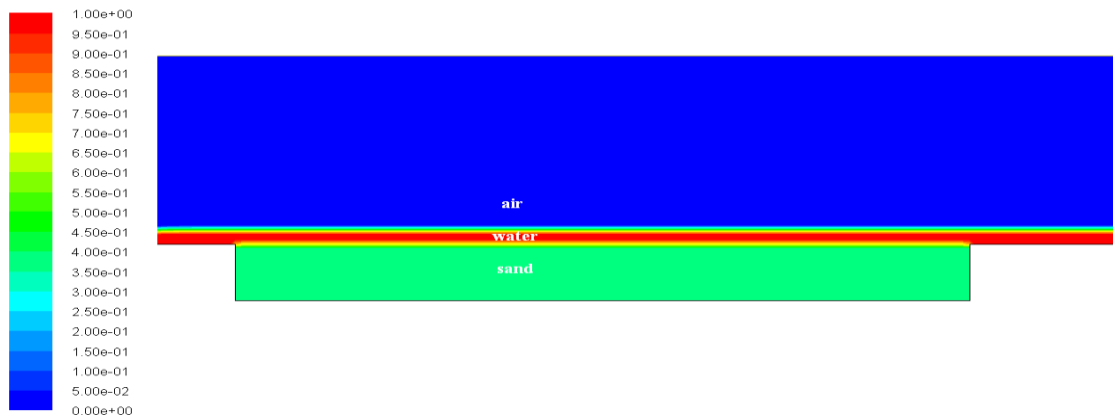


Figure 5.5 The contours of volume fractions at initial stage

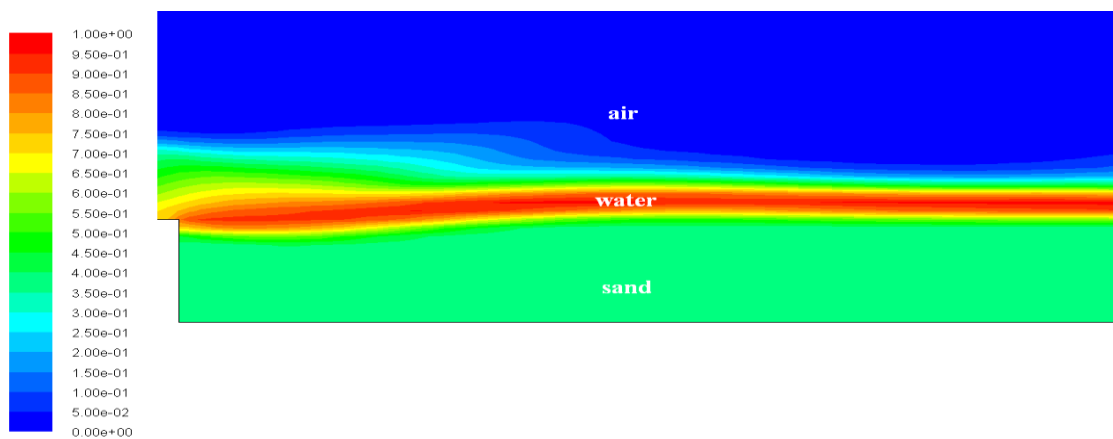


Figure 5.6 The contours of volume fractions of water phase for test 1

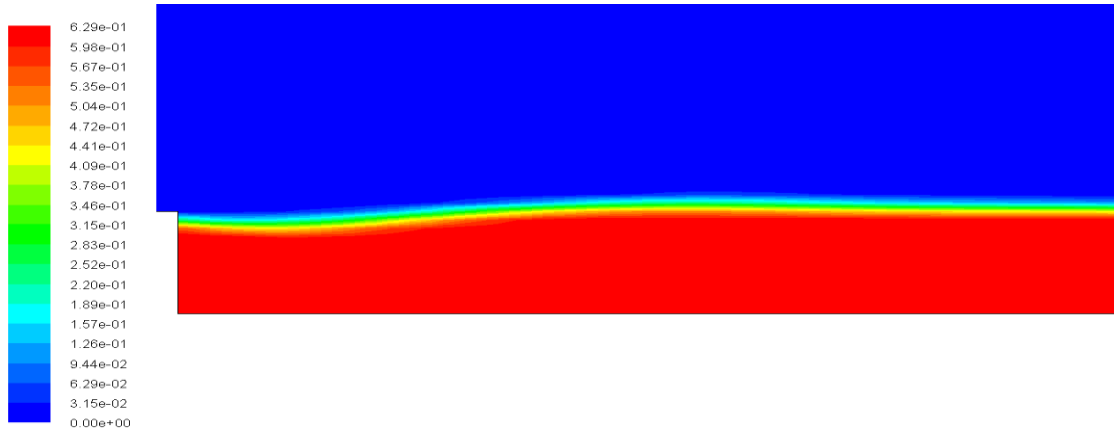


Figure 5.7 The contours of volume fractions of sand phase for test 1

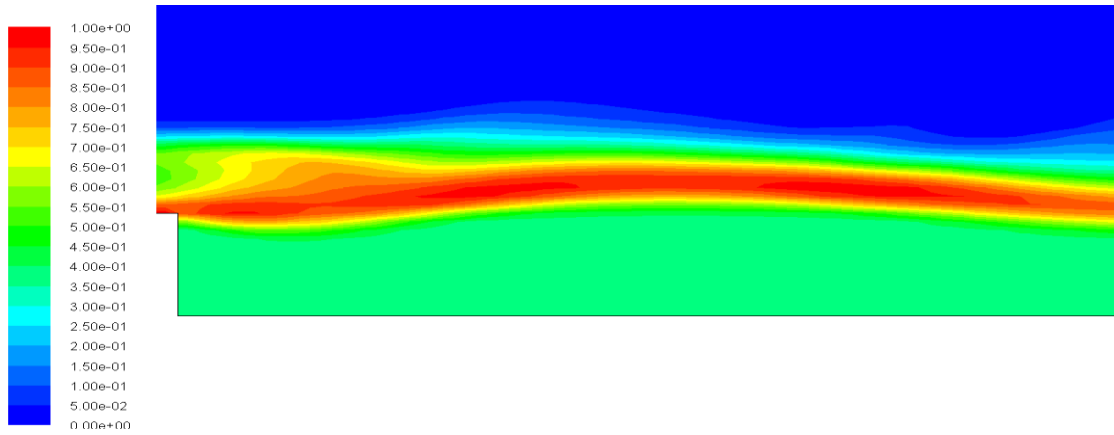


Figure 5.8 The contours of volume fractions of water phase for test 2

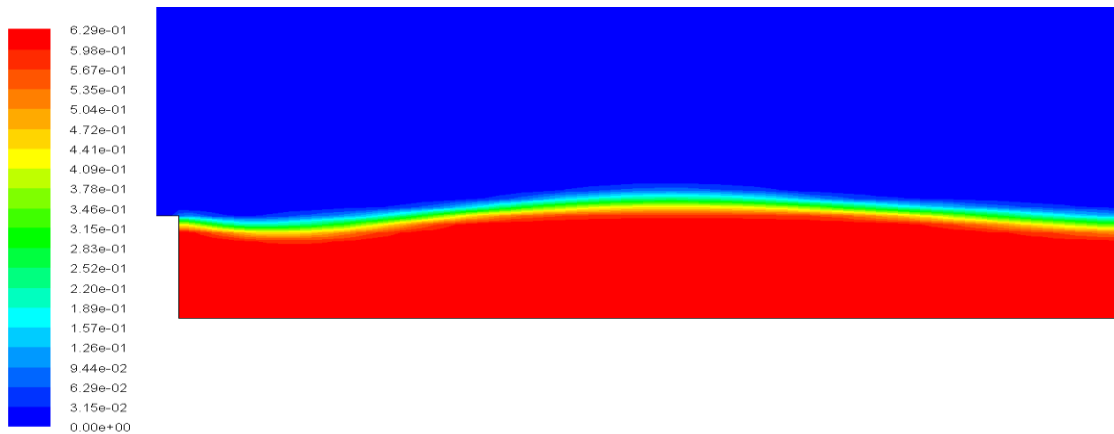


Figure 5.9 The contours of volume fractions of sand phase for test 2

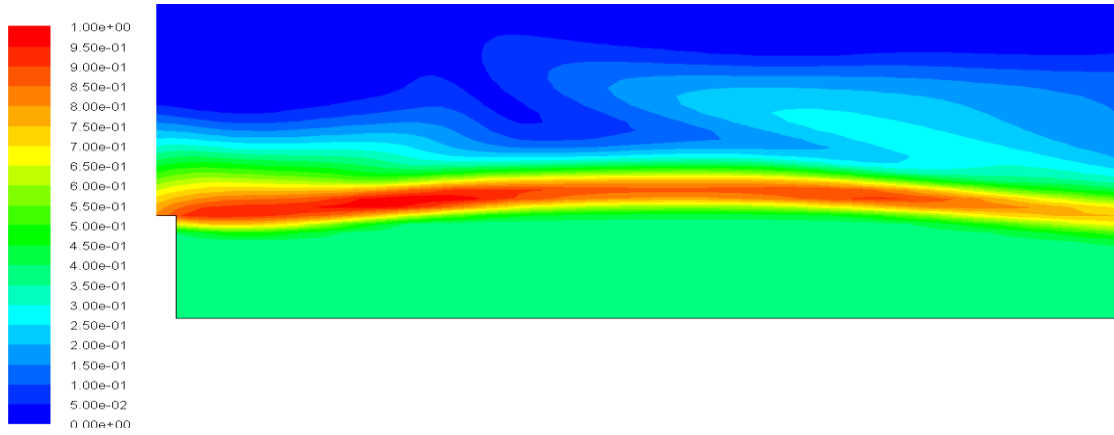


Figure 5.10 The contours of volume fractions of water phase for test 3

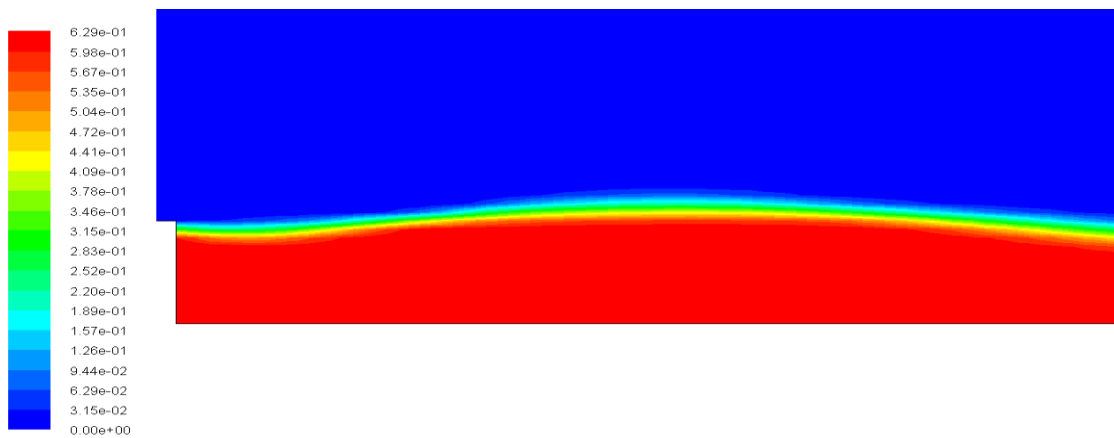


Figure 5.11 The contours of volume fractions of sand phase for test 3

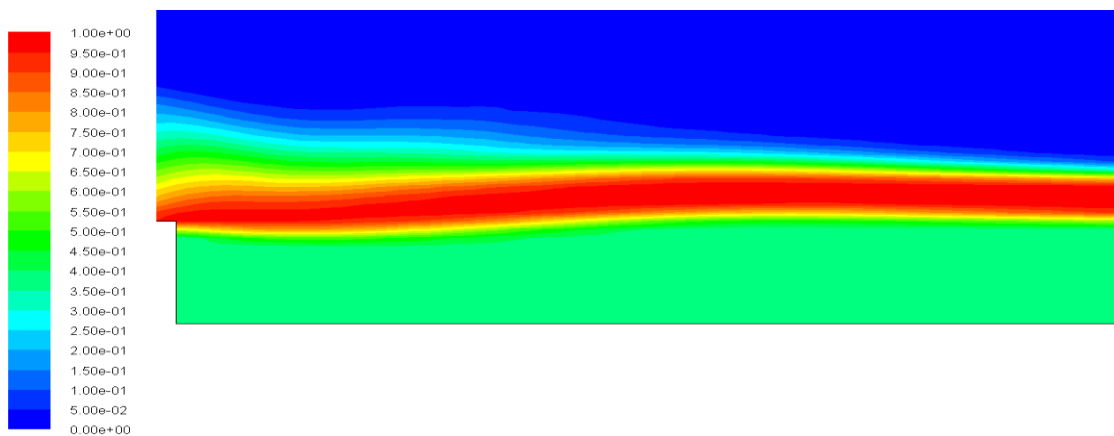


Figure 5.12 The contours of volume fractions of water phase for test 4

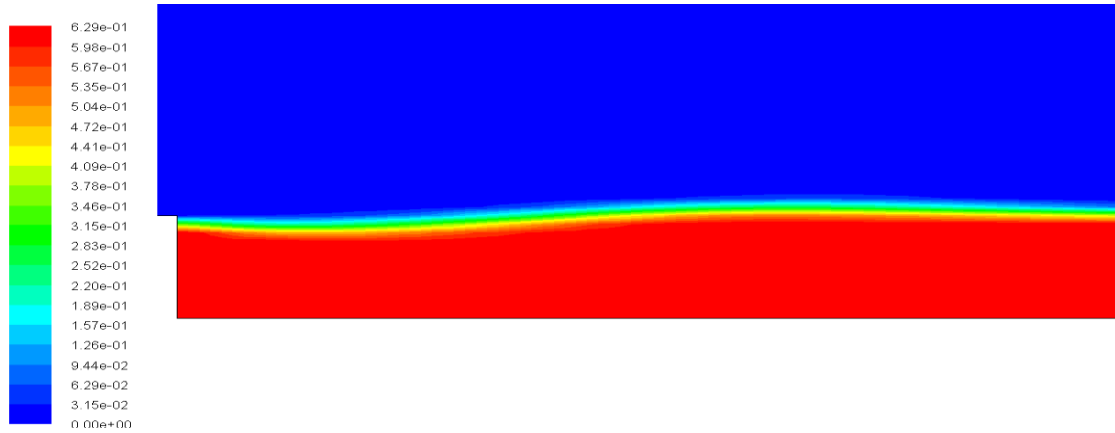


Figure 5.13 The contours of volume fractions of sand phase for test 4

The dune surface was observed to be not straight, as for the runs with smaller velocities, but there are various surges, which increase their length and amplitude with the increasing distance from the apron, related to an increase in the local velocity, due to the increasing dune height.

Figure 5.14-5.17 shows the predictions of water surface profile to the numerical ones measured by Fluent for tests 1, 2, 3 and 4, at asymptotic stages. At the inlet of the scour profile, the free surface profiles start to jump until a peak in the region of  $0 < x < 0.15$ . Downstream of this region ( $x > 0.1$ m), the flow decreases steadily, and then increases steadily reaching a smooth straight profile shape after  $x/h_s = 35$ .

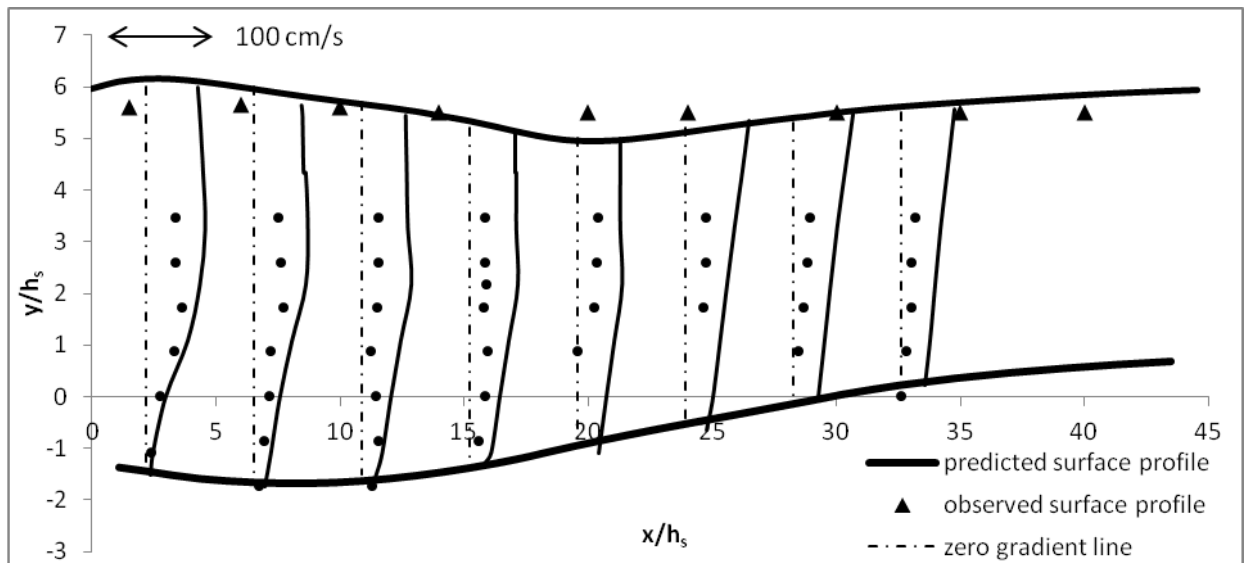


Figure 5.14 Distribution Fluent's  $u$ -velocity over the rigid apron and scour profile predictions for test 1.

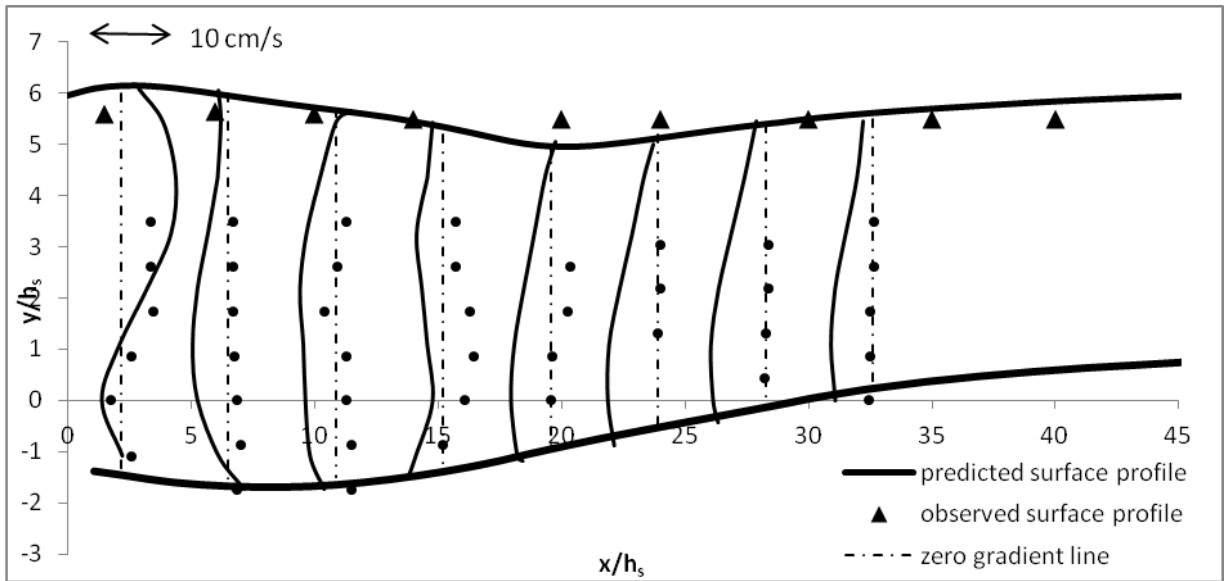


Figure 5.15 Distribution Fluent's  $v$ -velocity over the rigid apron and scour profile predictions for test 1.

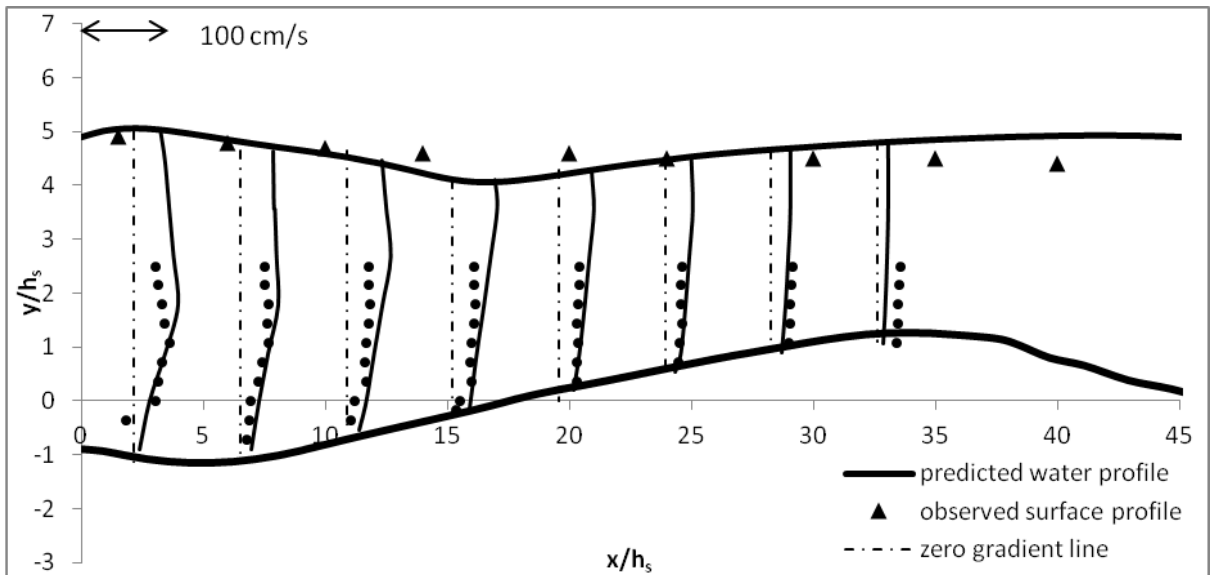


Figure 5.16 Distribution Fluent's  $u$ -velocity over the rigid apron and scour profile predictions for test 3.



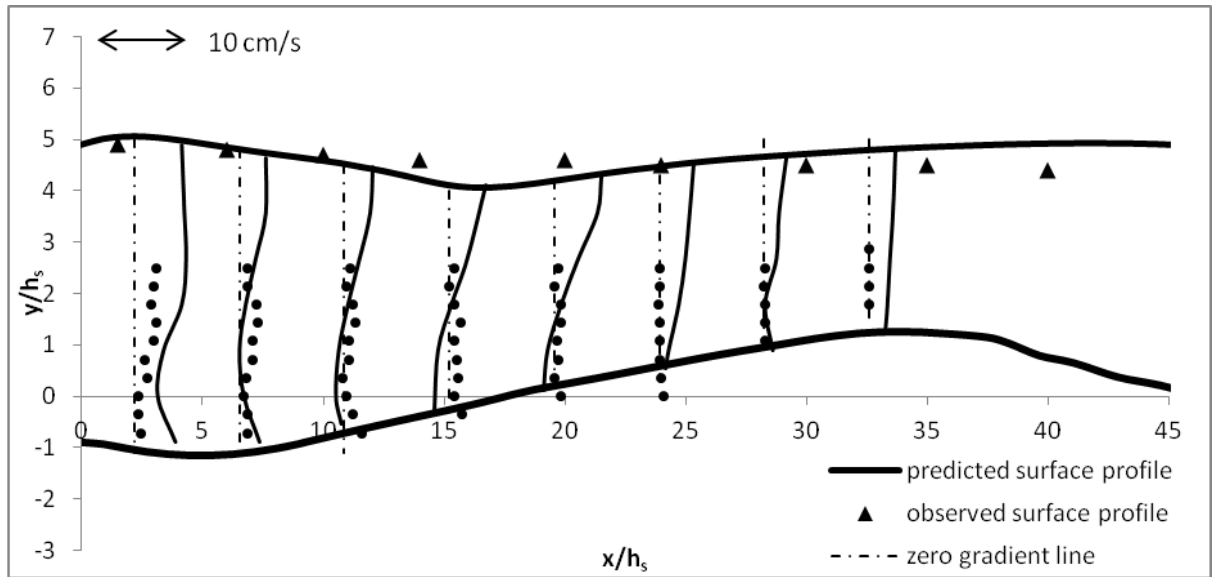


Figure 5.17 Distribution Fluent's  $v$ -velocity over the rigid apron and scour profile predictions for test 3.

The experimental velocity profiles ( $u, v$ ) for runs tests 1-4, measured by Adduce (2004) are compared with the numerical predictions of the proposed model in Figs. 5.14-5.21, respectively. In Figs. 5.14-5.21, the dots ( $\bullet$ ) symbolize the measured velocity, thick line illustrate the measured sand profiles and the thin black lines (-) represent the forecast of the present model to the measured ones. The velocity profiles shown in Figure 5.14-5.21 were positioned at  $x = 0.7, 0.8, 0.9, 1, 1.1, 1.2, 1.3$  and  $1.4$  m. From Figures 5.14–5.21, it is evident that the horizontal component ( $u$ ) of flow velocity is more high than the vertical one ( $v$ ) along the whole scour profile.  $h_s$  was used as a length scale of the horizontal and vertical distances. In Figures 5.14 and 5.16, for the test 1 and test 3, this can be detected that the maximum velocity increases from the maximum scour depth field to the peak point of dune, while it decreases beyond the peak point of the dune. As a general appearance, it can be concluded that the flow from the maximum scour depth to the end of the dune can be simulated by plane wall jet analogy (Narayanan, 1975).

Figures 5.18–5.21 illustrate the predictions of the present numerical model to the positional distribution of the Reynolds stresses ( $\sqrt{u'^2}, \sqrt{v'^2}$ ), for the tests 1-4 measured by Adduce (2004) using Micro Acoustic Doppler Velocimetry at the flume centreline. The triangles ( $\Delta$ ) delineate the measured surface profiles, dots ( $\bullet$ )

represent the measured velocity profiles and the solid lines (-) indicate the predictions of the present model to the measured ones. The Reynolds stress (35) made nondimensional by velocity scale  $U_0$  (defined in Equation (35)) and by the length scale  $y_0$  in horizontal plane.

$$U_0 = \frac{Q}{by_0}$$

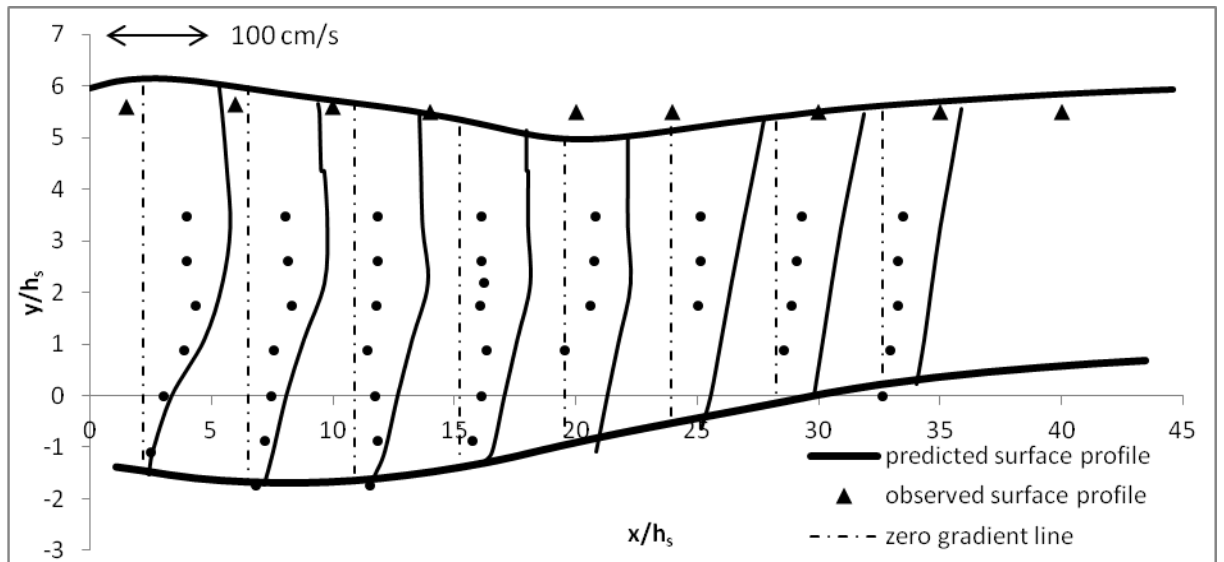


Figure 5.18 Predicted and observed  $\sqrt{U^2}/U_0$  distribution over the rigid apron and scour profile for test 1.

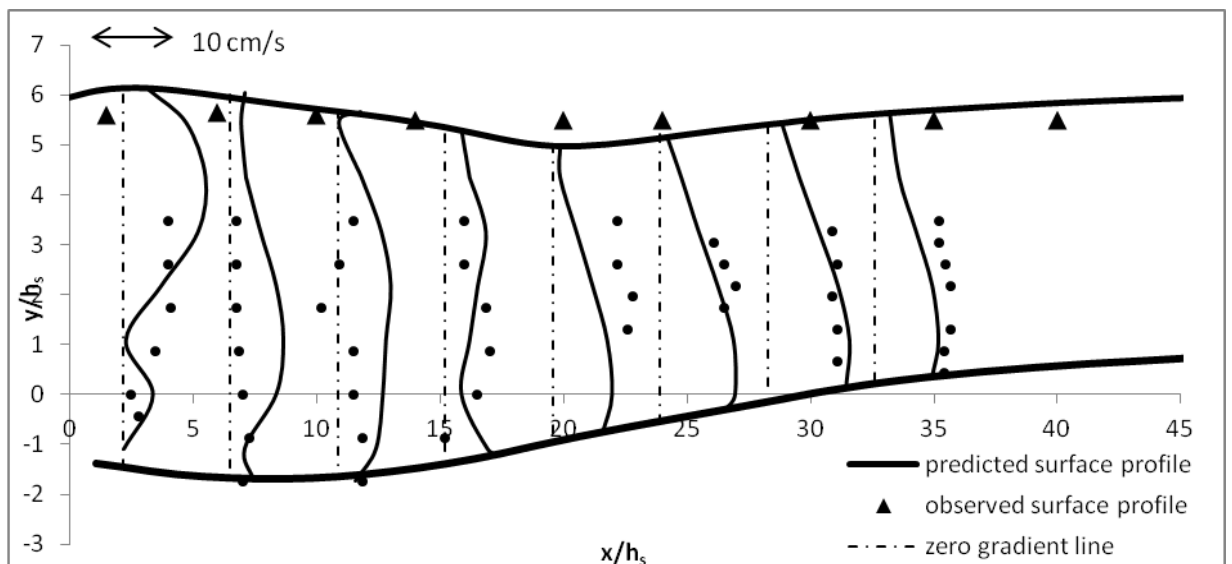


Figure 5.19 Predicted and observed  $\sqrt{V^2}/U_0$  distribution over the rigid apron and scour profile for test 1.

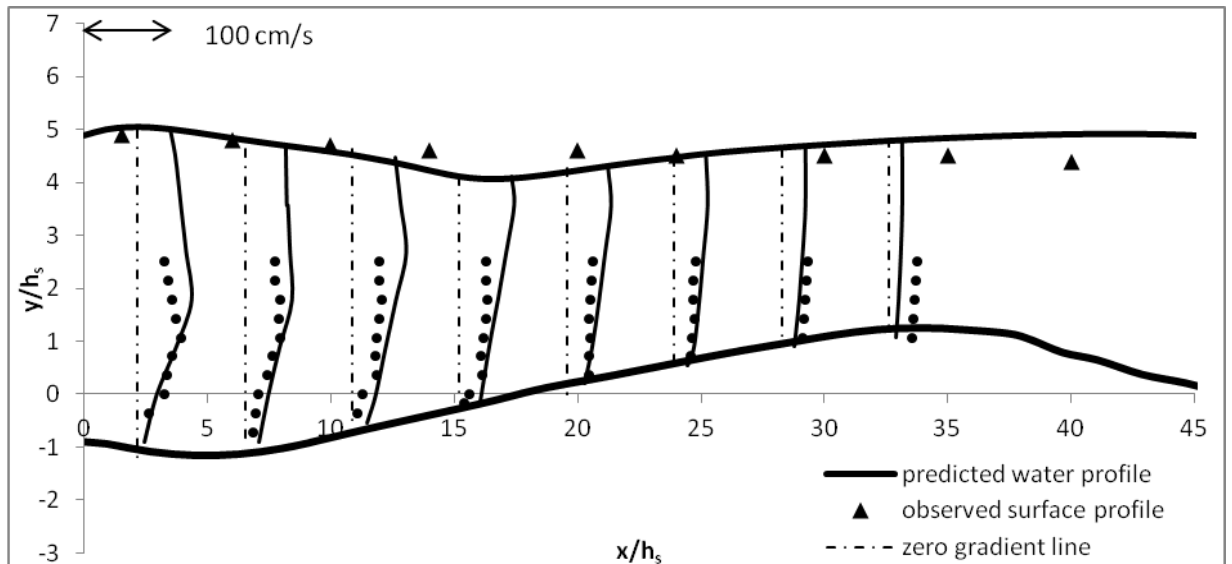


Figure 5.20 Predicted and observed  $\sqrt{U^2}/U_0$  distribution over the rigid apron and scour profile for test 3.

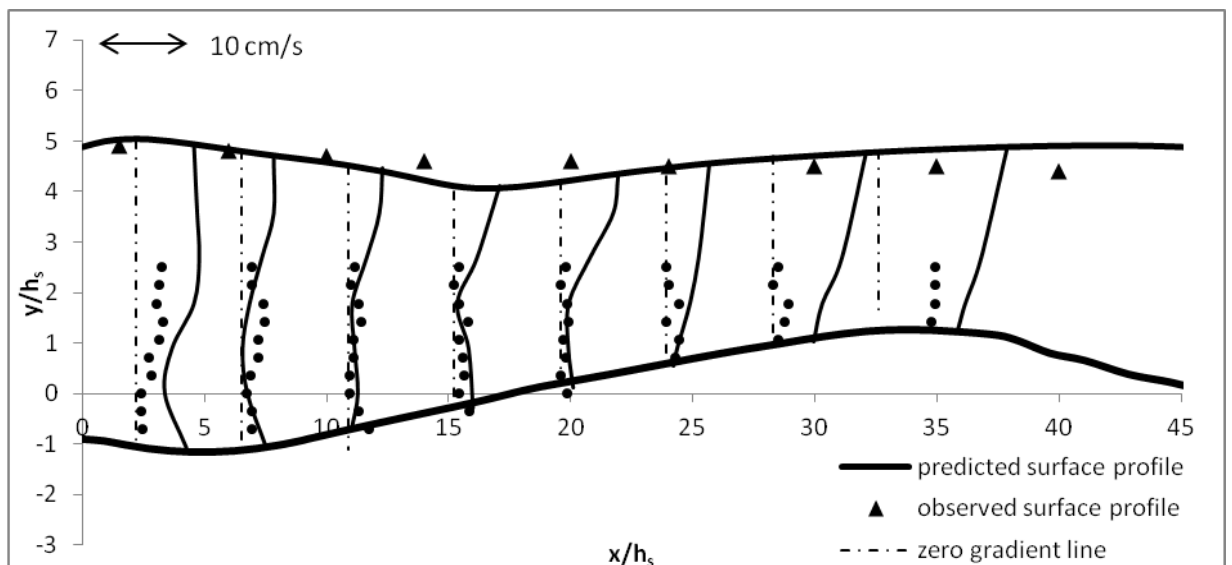


Figure 5.21 Predicted and observed  $\sqrt{V^2}/U_0$  distribution over the rigid apron and scour profile for test 3.

As a general view from Figures 5.18 and 5.20, as  $y/h_s$  increases,  $\sqrt{U^2}/U_0$  increases up to a maximum value, nearly at the point where the  $u$ -velocity distribution has also its maximum and then slightly reduces until the free surface. In the section between the maximum scour depths to the peak of dune, the  $\sqrt{U^2}/U_0$  distribution shows a

uniform profile. Both the measured and the predicted  $\sqrt{v'^2}$  values are obviously smaller than the corresponding  $\sqrt{u'^2}$  ones. This is a commonly expected case (Adduce, 2004; Guven, 2008; Guven and Gunal, 2009).

## CHAPTER 6

### CONCLUSIONS AND SUGGESTIONS FOR FURTHER RESEARCH

#### 6.1. Conclusions

In this study, numerical modeling of local scour beneath horizontal jets by developing a 3-phase mixture CFD model is presented. Different laboratory conditions were run to investigate local scour downstream of a threshold followed by solid apron using by FLUENT. The experimental data recorded by others are used for calibration and validation of the proposed numerical scheme.

FLUENT 6.3, a CFD package program was used to develop the proposed numerical scheme. Four test studies are executed. For each case study, several combinations were run by FLUENT and the settings which are thought to be the optimum ones are presented in this research.

The literature review showed that  $k - \epsilon$  turbulence model is so common performed to many engineering problems with good results. In this study, the RNG  $k - \epsilon$  model, which is an extension to the standard  $k - \epsilon$ , was used as the closure model. It was noted from the literature that RNG  $k - \epsilon$  is the most appropriate model concerning the scouring and complex-boundary turbulent flows.

For the pressure-velocity coupling is done by the Phase Coupled SIMPLE scheme. As an Eulerian model, the geometric reconstruction scheme of FLUENT is used, which gave the best results for the simulation of scour problem. For the calculation of scour a grid with 18099 quadrilateral cells were created. The time step size is set to 0.01 sec. The scour process improved rapidly during the beginning of the run and became slower and slower with time advance. The sand was drifted downstream by the water jet forming a dune, which increased its length and height with time advance.

## **6.2. Suggestions for further research**

The proposed model is under-estimated the turbulence parameters. This can be solved by calibration through applying the proposed model to different experimental case studies.

To improve the results obtained from FLUENT, user defined functions (UDFs) could be written and integrated into the program. The UDFs can be written in Visual C programming language. These UDFs can be used to define boundary conditions, material properties, and source terms for each special case, or to specify customized model parameters (e.g., DPM, multiphase models), initialize a solution, or enhance post-processing.

The capability of the proposed numerical model could be improved to be capable of simulating the local scour beneath other flow conditions such as offset or plunging jets, or downstream of breakwaters.

## REFERENCES

1. Abdelaziz, S., Bui, M. D., Rutschmann, P. (2010). Numerical simulation of scour development due to submerged horizontal jet. *River Flow 2010 - Dittrich, Koll, Aberle&Geisenhainer (eds)*
2. Abouzeid, G. A. A., Mohamed, H. I., Ali, S. M. (2006). 3-d numerical simulation of flow and clear water scour by interaction between bridge piers. *Tenth International Water Technology Conference. IWTC10 2006, Alexandria, Egypt*
3. Adduce, C. (2004). Local scour downstream of a turbulent jet. *Ph.D. Thesis, Department of Civil Engineering, University of Roma Tre, Italy, 2004.*
4. Ali, K. H. M., Karim, O. (2002). Simulation of flow around piers. *Journal of Hydraulic Research, Vol. 40, 2002*
5. Azhari et al. (2010). 3d numerical modelling of local scour around the cylindrical bridge piers. *XVIII International Conference on Water Resources CMWR 2010 J. Carrera (Ed) CIMNE, Barcelona 2010*
6. Azhari, A., Saghravani, S. F., Mohammadnezhad, B. A. (2010). 3d Numerical modelling of Local Scour Around The Cylindrical Bridge Piers. *XVIII International Conference on Water Resources CMWR. Barcelona*
7. Boussinesq, J. (1877). Essaisur la theorie des eauxcourantes, Mem. Ac.Sci.Inst.Nat. France XXIII, 1-680.
8. Bung et al. (2008). Bore propagation over a submerged horizontal plate by physical and numerical simulation. *International Conference on Coastal Engineering (ICCE). 31.08.-05.09.2008, Hamburg.*
9. Cassan, L., Belaud, G. (2011). Experimental and numerical studies of the flow structure generated by a submerged sluice gate. UMR G-EAU, Cemagref/IRD/Supagro, Montpellier, France,
10. Castillo, L. G., Carrillo, J. M. (2011). Numerical simulation and validation of hydrodynamics actions in energy dissipation devices. *Technical University of Cartagena Paseo Alfonso XIII, 52, 30203 Cartagena SPAIN*
11. Chang, H. T. (1977). Vortex Scour Due to Wave Action at a Breakwater Tip. *6th Australasian Hydraulics and Fluid Mechanics Conference Adelaide, Australia, 5-9 December 1977*

12. Chen, B. (2006). The numerical simulation of scour in front of a vertical wall breakwater. *Journal of hydrodynamics*, 18, 3.
13. Chen, B., Cheng, L. (2002). Numerical Investigation of Three-dimensional Flow around a Free-Spanned Pipeline. *Proceedings of The Twelfth (2002) International Offshore and Polar Engineering Conference Kitakyushu, Japan, May 26-31, 2002*
14. Creaco, E., Bertrand-Krajewski, J. L. (2007). Modelling the flushing of sediments in a combined sewer. *Proceedings of Novatech2007*, Lyon, France, 24-27 June
15. Dargahi, B. (2003). Scour development downstream of a spillway. *Journal of Hydraulic Research*. 41(4), 417-426.
16. Duc, B. M., Wenka, T., Rodi, W. (2004). Numerical Modeling of Bed Deformation in Laboratory Channels. *Journal of Hydraulic Engineering*, September 2004, 894-904.
17. Esmaili, T., Dehghani, A. A., Zahiri, A. R., Suzuki, K. (2009). 3d Numerical Simulation of Scouring Around Bridge Piers (Case Study: Bridge 524 crosses the Tanana River). *World Academy of Science, Engineering and Technology* 58
18. Fard, M. G., Yeganeh-Bakhtiary, A., Cheng, L. (2005). Two-phase flow modeling of clear-water onset and jet scour under offshore pipelines. *Proceeding XXXI IAHR Congress, pp. 4069-4080*, Seoul, Korea
19. Fluent User Guide. (2001). "*FLUENT 6.0 User' Guide*"
20. Guney, M. S., Aksoy, A. O., Bombar, G. (2011). Experimental Study of Local Scour Versus Time Around Circular Bridge Pier. *6th International Advanced Technologies Symposium (IATS'11). 16-18 May 2011, Elazığ, Turkey*
21. Guven, A., Gunal, M. (2009). Hybrid modelling for simulation of scour and flow patterns in laboratory flumes. *Int. J. Numer. Meth. Fluids*, DOI: 10.1002/flid.2022.
22. Hajivalie, F., Yeganeh-Bakhtiary, A. (2009). Numerical Study of Breakwater Steepness Effect on the Hydrodynamics of Standing Waves and Steady Streaming. *Journal of Coastal Research, SI56, 514-518*, Lisbon, Portugal
23. Hanjalic, K., Launder, B.E., (1972). A Reynolds stress model of turbulence and its application to thin shear flows. *J. Fluid Mech.* 52, pp.609–638
24. Harb, G., Zeng, G. (2011). Customized informatics tools for the hydropower reservoir management optimization, concerning sediment management and hydraulic modeling. *South-East-Europe Transnational Cooperation Programme*



25. Hargreaves, D. M., Morvan, H. P., Wright, N. G. (2007). Validation of the volume of fluid method for free surface calculation: the broad-crested weir. *Engineering Applications of Computational Fluid Mechanics Vol. 1, No. 2, pp. 136–146* (2007)
26. Harlow, F. H., Nakayama, P.I. (1968). Transport of turbulence energy decay rate. *LA-3854, Los Alamos Science Lab., U. California, USA.*
27. Hassan, N.M.K., Narayanan, R. (1985). Local scour downstream of an apron. *J. Hydr. Engrg., ASCE, 111(11), pp 1371–1385*
28. Heather, D. S. (2004). Modelling the flow and scour around an immovable cylinder. *Master thesis. Department of Civil Engineering, The Ohio State University*
29. Hogg, A. J., Pritchard, D. (2004). The transport of sediment over a sloping breakwater. *15th Australasian Fluid Mechanics Conference The University of Sydney. Sydney, Australia 13-17 December 2004*
30. Hughes, S. A., Schwichtenberg, B. R. (1998). Physical Model of Current-Induced Scour at Ventura Harbor. *Proceedings of Breakwater '99 Conference, American Society of Civil Engineers*
31. Iyalla, I., Umah, K., Hossain, M. (2010). Computational Fluid Dynamics Modelling of Pipe-Soil Interaction in Current. *Proceedings of the World Congress on Engineering 2010 Vol II WCE 2010, June 30 - July 2, 2010, London, U.K.*
32. Jensen et al. (1990). Flow around and forces on a pipeline near a scoured bed in steady current. *J. Offshore Mech. Arct., 112:206–213*
33. Kalin, L., Hantush, M. M. (2003). Evaluation of sediment transport models and comparative application of two watershed models. *EPA Report No. EPA/600/R-03/139, USEPA-NRMRL, Cincinnati, OH*
34. Karim, O. A., Ali, K. H. M. (2000). Prediction of Flow Patterns in Local Scour Holes caused by Turbulent Water Jets. *Journal of Hydr. Research. Vol.38 pp.279-287.*
35. Kolmogorov, A. N. (1942). Equations of motion of an incompressible turbulent fluid. *IzvAkadNauk SSSR SerPhys VI No 1-2, p56*
36. Lauck, T., Lamberson, R., Lisle, T. E. (1993). A simulation model for the infiltration of heterogeneous sediment into a stream bed. *In: Advances in Hydro-Science and Engineering, Vol. 1, S.S.Y. Wang (ed.), p. 229-236*
37. *Launder, B.E. and Spalding, D.B. (1974), "The numerical computation of turbulent flows. Computer Methods in Applied Mechanics and Engineering, 3 (2): 269-289,*

38. Lohász, M., Csécs, Á. (2003). Rans computation of ribbed duct flow using fluent and comparing to les. *Department of Fluid Mechanics, Budapest University of Technology and Economics, Budapest*
39. Lu et al. (2005). Numerical simulation of the equilibrium profile of local scour around submarine pipelines based on renormalized group turbulence model. *Ocean Engineering* 32 (2005) 2007–2019
40. Lu, Y. (2007). Numerical simulation of two-dimensional overtopping against seawalls armored with artificial units in regular waves. *Journal of Hydrodynamics Ser.B, 2007,19(3):322-329*
41. Manninen, M., Taivassalo, V. (1996). On the mixture model for multiphase flow. *ValtionTeknillinenTutkimuskeskus. Espoo 1996.*
42. Mashriqui, H. S. (2003). Hydrodynamic and Sediment Transport Modeling of Deltaic Sediment Processes. *Ph.D. Dissertation. Louisiana State University, Department of Civil and Environmental Engineering. Baton Rouge, Louisiana*
43. Pasiok, R., Stilger-Szydło, E. (2010). Sediment particles and turbulent flow simulation around bridge piers. *Archives of civil and mechanical engineering Vol.X, No.2*
44. Patankar, S. V. (1980). Numerical Heat Transfer and Fluid Flow. *Hemisphere Publishing Corp., Washington, DC 1980.*
45. Rajaratnam, N. (1981). Erosion by plane turbulent jets. *Journal of Hydraulic Research, 19, 339-358.*
46. Rodi W.,(1980). Turbulence Models and Their Application in Hydraulics - a State of the Art Review, University of Karlsruhe, Karlsruhe, Germany.
47. Sarkar, M.A., Rhodes, D.G. (2004). Calculation of free-surface profile over a rectangular broad-crested weir. *Flow Measurement and Instrumentation* 15:215–219
48. Shen, Y., Liu, C. (2009). A three-dimensional  $k-\varepsilon$  - $k-p$  model in curvilinear coordinates for sediment movement and bed evolution. *Sci China Ser E-Tech Sci* April 2009, vol. 52, no. 4, 1090-1100
49. Smith, H. D. (2004). Modelling the flow and scour around an immovable cylinder. *Presented in Partial Fulfillment of the Requirements for the Degree Master of Science in the Graduate School of The Ohio State University*
50. Stoesser, T. (1999). On the use of a 3d CFD model to simulate reservoir sedimentation processes. *Proceedings of the XX IAHR Conference Graz, Austria, 1999*

51. Stoesser, T., Fröhlich, J., Rodi, W. (2006). Large eddy simulation of open-channel flow over and through two layers of spheres. *The 7th Int. Conf. on Hydroscience and Engineering (ICHE-2006)*, Sep. 10 – Sep. 13, Philadelphia, USA
52. Symlal, M., O'Brien, T. J. (1989). Computer simulation of bubbles in a fluidized bed. *AIChE Symposium Series*, 85 (1989), pp. 22–31
53. Teruzzi et al. (2006). Numerical investigation of the turbulent flow around a bridge abutment. *River Flow 2006 – Ferreira, Alves, Leal & Cardoso (eds) © 2006 Taylor & Francis Group, London, ISBN 0-415-40815-6*
54. Uyumaz, A., (1988). Scour downstream of vertical gate. *J. HydrEngrg., ASCE*, 114(7), pp 811–816
55. Van Beek, F. A. Wind, H. G. (1990). Numerical Modelling of Erosion and Sedimentation Around Offshore Pipelines. *Coastal Engineering*, 14 (1990) 107-128 Elsevier Science Publishers B.V., Amsterdam -- Printed in The Netherlands
56. Vasquez, J. A. Walsh, B. W. (2009). CFD simulation of local scour in complex piers under tidal flow. *33rd IAHR Congress: Water Engineering for a Sustainable Environment*
57. Vasquez, S. A., Ivanov, V. A. (2000). A Phase Coupled Method for Solving Multiphase Problems on Unstructured Meshes. *ASME FEDSM'00: ASME 2000 Fluids Engineering Division Summer Meeting*.
58. Versteeg, H.K., Malalasekera, W. (1995). Introduction to computational fluid dynamics. The finite volume method (Longman)(T)(ISBN 0582218845)
59. Vuik, V. (2010). Numerical modeling of sediment transport over hydraulic structures. *Delft University of Technology Faculty of Civil Engineering and Geosciences Section of Hydraulic Engineering Field of River Engineering*
60. Wang, S., Wu, W. (2004). River sedimentation and morphology modeling – the state of the art and future development. *Proceedings of the Ninth International Symposium on River Sedimentation*. October 18 – 21, 2004, Yichang, China
61. Weiss, J. M., Maruszewski, J. P., Smith, W. A. (1999). Implicit Solution of Preconditioned Navier-Stokes Equations Using Algebraic Multigrid. *AIAA Journal*, **37**, 29-36.
62. Wilcox, D., (1988). Reassessment of the Scale Determining Equation for advanced Turbulence Models, *AIAA J.*, Vol. 26, No. 11, pp 1299-1310.
63. Yakhot, V., Orszag, S.A., (1986). Renormalization group analysis of turbulence. *Journal of Scientific Computing*.

64. Yang, Q. (2005). Numerical investigations of scale effects on local scour around a bridge pier. *Department of Civil and Environmental Engineering In partial fulfillment of the Requirements for the degree of Master of Science*
65. Yeganeh-Bakhtiary, A., Kazeminezhad, M. H., Etemad-Shahidi, A. (2011). Euler–Euler two-phase flow simulation of tunnel erosion beneath marine pipelines. *Applied Ocean Research* 33, 2011
66. Zaredehdasht et al. (2011). An Examination of the Water Erosion Incursion In too the Bridge Pillars Through the Method of Slipping the Pillars Using the Numerical Model of Data Analysis of Fluent. *Australian Journal of Basic and Applied Sciences*, 5(9): 13-21, 2011 ISSN 1991-8178
67. Zhang et al. (2005). Three-dimensional mathematical modeling of local scour. *Journal of Applied Mechanics Vol.8*
68. Zhang, H., Nakagawa, H., Kawaike, K., Baba, Y. (2009). Experiment and simulation of turbulent flow in local scour around a spur dyke. *International Journal of Sediment Research*, **24**, 33–45.